NATIONAL ADVISORY COMMITTEE
FOR AERONAUTICS

TECHNICAL NOTE 3723

CALCULATIONS OF THE FLOW OVER AN INCLINED FLAT PLATE

AT FREE-STREAM MACH NUMBER 1

By Walter G. Vincenti, Cleo B. Wagoner, and
Newman H. Fisher, Jr.

Ames Aeronautical Laboratory
Moffett Field, Calif.

NACA

Washington
August 1956

.V

NATIONAL ADVISORY COMMITTEE FOR AERONAUTICS

TECHNICAL NOTE 3723

CALCULATIONS OF THE FLOW OVER AN INCLINED FLAT PLATE

AT FREE-STREAM MACH NUMBER 1

By Walter G. Vincenti, Cleo B. Wagoner, and
Newman H. Fisher, Jr.

SUMMARY

A numerical solution has been obtained of the complete equations of inviscid compressible flow for the case of an inclined flat plate at free-stream Mach number 1. The mixed flow about the lower surface of the plate is found by relaxation solution of a boundary-value problem in the hodograph plane. Considerable preliminary analysis is required by the presence of the free-stream singularity, which must be incorporated analytically into the numerical work. The methods devised for this part of the work may have application in other problems of transonic flow. The supersonic flow on the upper side of the plate is found in the physical plane by a standard form of the method of characteristics. The calculations here are carried only as far as the end of the separated region that appears on the upper surface near the leading edge. The results, which are for an angle of attack of 13°, show the pressure distribution on the lower surface and the detailed flow field about the lower surface and the leading edge.

The results for the flow field show that the large changes of velocity that occur near the leading edge are confined to a surprisingly small part of the field. The stagnation point on the underside of the plate, for example, is found to be only 0.0016 of the chord aft of the leading edge. (This is in contrast to a value of 0.05 for incompressible flow about a plate at the same angle of attack.) The average radius of curvature of the sonic line as it approaches the leading edge is even smaller. To see the details here, in fact, it is necessary to plot the results to a scale in which the displacement of the stagnation point aft of the leading edge is approximately 50 inches.

The calculations of the pressure distribution indicate that Guderley's earlier solution on the basis of the transonic small-disturbance theory gives reasonably accurate results even at the present moderately large angle of attack. If the small-disturbance values are corrected by a method due also to Guderley, the error is almost completely eliminated except at the leading edge where the corrected solution still cannot represent the true flow.

INTRODUCTION

The problem of the two-dimensional flow over an inclined flat plate at free-stream Mach number 1 has been discussed by Guderley in reference 1. This problem is of interest as an example of the unsymmetric transonic flow that occurs around a sharp-nosed airfoil when the angle of attack is large compared with the nose angle. (On a plate, where the nose angle is zero, any angle of attack meets this description.) A solution of the problem was given by Guderley on the basis of the small-disturbance theory for transonic flow. This solution, arrived at by an ingenious analytical procedure, gives useful information on the pressure distribution on both surfaces of the plate. Owing to the approximations involved in the theory, however, the results are limited to angles of attack which, though large in comparison with the nose angle, are in themselves still small. More important, the details of the flow at the leading edge, which are of fundamental interest, do not appear in the analysis.

The work to be described in the present paper was conceived as part of a study of the transonic flow around leading edges. To supply the details missing in the small-disturbance analysis, it is proposed here to solve the flat-plate problem using the complete equations of inviscid compressible flow. The exclusion of viscosity may, it is realized, lead to some error at the sharp leading edge. If past experience is any guide, however, an inviscid solution will be of value toward understanding the actual viscous flow. It will also provide, for one specific case, a check of the accuracy of a known small-disturbance solution.

Since the analytical problem for the complete equations is a formidable one, the solution in the present work is carried out largely by numerical means.[1] As in Guderley's analysis, the mixed flow over the lower surface of the plate is found by solution of a boundary-value problem in the hodograph plane. The only real difficulty here is with the free-stream singularity, which must be incorporated analytically into the numerical work. The numerical procedures themselves are an extension of the work already reported in references 3 and 4. The supersonic flow on the upper side of the plate is found in the physical plane by the method of characteristics. In the present report this part of the calculation is carried only as far as the end of the closed region of separation that appears on the upper surface adjacent to the leading edge. It is hoped eventually to complete the solution to the trailing edge, but owing to circumstances outside the work this will not be possible in the immediate future.

The calculated results, which are for an angle of attack of 13°, show the pressure distribution on the lower surface and the flow field about the

---

[1]The analytical solution of the two-dimensional airfoil problem for the complete equations has been treated by Frankl in reference 2, which came to the authors' attention after the present work was under way. Frankl gives a general solution in the form of an infinite series of Chaplygin solutions. The application of this general solution to a specific boundary-value problem, however, is not discussed.

lower surface and the leading edge. In view of the known properties of flows near the sonic flight speed (see refs. 5 and 6), the results should be applicable for a range of free-stream Mach number either side of 1. This is especially true of the flow in the immediate vicinity of the leading edge. Because of the nature of the flow field, the findings for the lower surface of the plate can be applied, within minor limitations, to the flow on the underside of any sharp-nosed airfoil with a flat lower surface.

As in reference 3, the report is divided into two parts. Part I contains an outline of the general problem and its solution and a discussion of the final results. Part II supplies the mathematical details. A summary of the notation is given in an appendix at the end of the report.

The relaxation calculations for the lower surface of the plate were performed with unusual skill and diligence by Mrs. Marjorie Sill. The characteristics construction on the upper surface was programmed for the electronic computer by Meyer M. Resnikoff, who contributed many valuable ideas to this phase of the work.

I - GENERAL PROBLEM AND FINAL RESULTS

GENERAL PROBLEM

Description of Flow Field

The inviscid flow over an inclined plate at free-stream Mach number 1 has been described by Guderley in reference 1. A qualitative picture of the flow is given in sketch (a), which is essentially a reproduction of figure 1 of Guderley's report.

As shown in the sketch, there exists at angle of attack a large region of subsonic flow in front of and beneath the plate. This region is bounded by the lower surface DB of the plate, by sonic lines DO and BO springing from the leading and trailing edges, and by the free stream O at infinity. In this region, as in incompressible flow, the fluid forward of the plate is deflected upward. As a result, a stagnation point C occurs on the lower surface

Sketch (a)
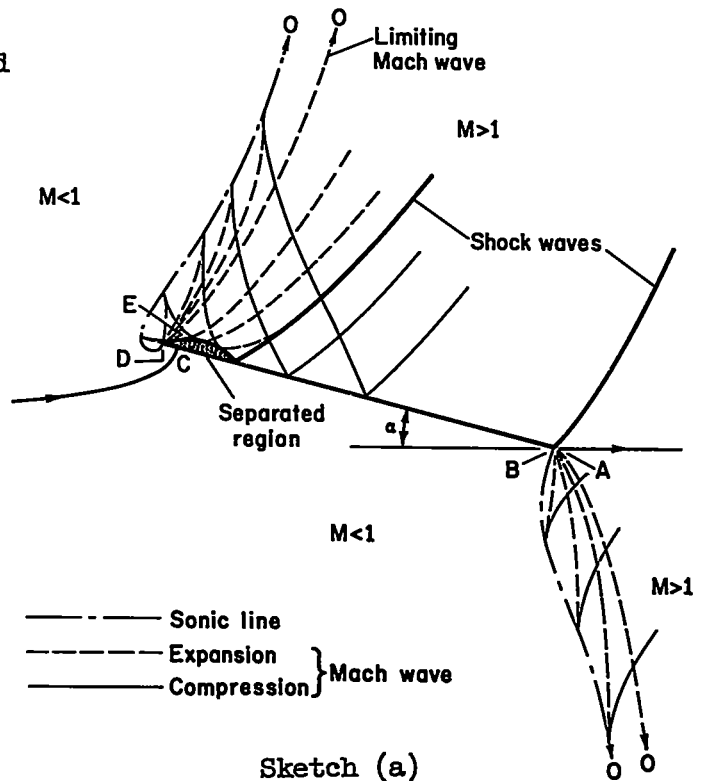
of the plate near the leading edge. At this point the central (or "stag-
nation") streamline branches to run both fore and aft along the plate.
Sonic speed is reached on the surface of the plate precisely at the lead-
ing and trailing edges D and B. The sonic line from each of these edges
leaves the plate at right angles to the lower surface. Downstream of each
sonic line there occurs a supersonic expansion fan centered at the edge.

Expansion fans of the type encountered here have been described in
detail in references 3 and 7. In the limit of the edge itself, the fan
approaches the classical Prandtl-Meyer flow. Away from the edge, however,
the elementary expansion waves (or Mach waves), which are straight in the
Prandtl-Meyer case, now bend upstream toward the sonic line. Some of
these expansion waves, in fact, meet the sonic line, where they are
reflected as compressions; others pass entirely downstream of the line.
The wave that separates the two classes of expansion waves, the so-called
"limiting wave" (see EO and AO in sketch (a)), approaches the sonic line
at infinity. Obviously - and this is the essential point - the flow in
the subsonic region must depend in part on conditions in the supersonic
fan ahead of the limiting wave. It is, however, completely independent
of conditions downstream of this wave.

The details of the flow over the upper surface of the plate are not
completely certain. Even in the absence of viscosity, a separated region
must be expected adjacent to the leading edge. This follows from the
fact that the angle of turn called for at the edge - 180° in the present
case - is greater than the 130° attainable by expansion to a vacuum. In
any real fluid, of course, the pressure actually attained in the separated
region will be fixed by viscous phenomena. From the standpoint of the
present purely inviscid theory, however, this pressure is to be regarded
as an assignable parameter (subject to one restriction to be mentioned
later). Once the flow has separated from the plate, the central stream-
line follows a path of constant pressure. To do this in the presence of
the compression waves reflected from the sonic line, it must curve back
again toward the plate. At some point the streamline will presumably
reattach to the plate and be deflected to the direction of the upper sur-
face by an oblique shock wave. Downstream of this reattachment wave, the
flow will proceed at decreasing supersonic speed to the trailing edge,
where a second shock wave will occur. The foregoing is, at least, a
plausible description of the flow as it might be expected to exist on the
upper surface. It is not inconceivable, however, that the shock system
could be more complicated than that described here.

The foregoing discussion implies one restriction that has not yet
been stated. This is that the pressure assigned in the separated region
must be not greater than that which exists where the limiting wave meets
the leading edge. For pressures greater than this value, the limiting
wave would have to start, not at the leading edge, but at some point on
the separated streamline. In this situation the part of the streamline
between the leading edge and the foot of the limiting wave would be inter-
dependent with the subsonic field. The problem would then be slightly
different from that considered here, though the methods devised in this

report could again be used to obtain a solution. Since the flow on the underside of the plate would be little affected in any event, this second possibility will be ignored, and the earlier situation will be presumed to exist.

As should be apparent from this discussion, the analytical problem falls into two parts. To calculate the flow on the lower surface of the plate, a transonic boundary-value problem must be solved in a region consisting of the subsonic field and those portions of the two supersonic fans ahead of their limiting waves. Once conditions on the upper limiting wave are known, the calculation of the field above the plate is an initial-value problem in purely supersonic flow. In the first problem, the flow is everywhere irrotational. In the second problem, it is irrotational as far as the reattachment wave and rotational after that.

Method of Analysis

The method of analysis is described in detail in part II of the report. The mixed flow about the underside of the plate is found by numerical (i.e., finite-difference) solution of a boundary-value problem in the hodograph plane. In this formulation of the problem, the free stream appears as a singularity - that is, an infinity - at a point on the sonic circle. This singularity consists of two superposed parts, one antisymmetric and similar to a doublet, the other symmetric and similar to a vortex. To calculate the flow, two separate boundary-value problems are solved, each containing one of the elementary singularities. The final result is then obtained by combining the two solutions to meet the condition that the central streamline branches at the stagnation point.

As in all finite-difference work, the singularities must be incorporated into the solutions analytically. This is complicated in the present case by the fact that simple closed expressions for the singularities are not available for the complete differential equation. A suitable method can be devised, however, based on the use of known results for the Tricomi equation. The method takes full account of the primary effect of the singularity. A small approximation is involved, however, in that singularities in certain of the higher-order derivatives (i.e., second order and above) are ignored in the numerical calculations. Experience indicates that the error from this source is probably smaller than that involved in the finite-difference process itself. It is sure to be negligible in the vicinity of the plate.

The finite-difference solution of the boundary-value problems entails several elements of novelty. These are made necessary by the presence of the singularity and by the mixed nature of the flow field. In the subsonic region the finite-difference equations are established in what is essentially a polar coordinate system. Except for the inclusion of the singularity, the procedures here are more or less standard. In the supersonic region the equations are set up in characteristic coordinates. The procedures here and at the transition from one coordinate system to the

other at the sonic line are somewhat unusual. Solution of the system of finite-difference equations is carried out on desk calculators by a combination of relaxation techniques and step-by-step procedures. Once the solution is obtained in the hodograph plane, transformation to the physical plane is a simple matter.

The purely supersonic flow over the upper surface of the plate is found in the physical plane by a standard form of the method of characteristics. In the present work a completely numerical process was used, in contrast to the more usual semigraphical procedures. This was done for two reasons: (1) The high Mach numbers and correspondingly small Mach angles in the vicinity of the separated region made any semigraphical procedure of doubtful accuracy; and (2) the large number of points required in the characteristics net made the use of automatic computing machines mandatory. The numerical work was carried out on an electronic digital computer. As mentioned in the introduction, the calculations for this part of the problem have been carried only as far as the reattachment point on the upper surface. For the time being they have also been confined to only one value of the separation pressure. It is hoped that the work can be carried on to the trailing edge and repeated for other values of the separation pressure at a later date.

RESULTS AND DISCUSSION

Calculations have been made, on the basis of the methods outlined, for an angle of attack of 13°. The work was carried out for a ratio of specific heats γ of 1.405 instead of the more usual value of 7/5. This was done because it was originally intended that the characteristics construction would be made by a semigraphical version of Guderley's method, for which extensive tables on the basis of the former value are available (ref. 8). When this method was abandoned in favor of automatic numerical computation (which does not utilize the tables), the calculations for the lower surface with $\gamma = 1.405$ were too far along to alter. The final results in the physical plane are shown in figures 1 and 2 and are discussed in the following paragraphs. (For results in the hodograph plane, see part II of the report.)

Flow Field

Lower surface and leading edge.- The flow field about the lower surface and leading edge is shown in figures 1(a) through 1(d). To understand these figures, it will perhaps be best to follow them through consecutively in some detail.

The first figure (1(a)) shows the complete plate from the leading edge to the trailing edge. In this and the subsequent parts of figure 1, size is indicated by a scale of s/c, where s is any length in the field

and c is the chord of the plate. Streamlines are identified by a value
of $[\delta(y/c)]_\infty$, which denotes the vertical distance at infinity between the
streamline in question and the central (or stagnation) streamline. Con-
tours of constant fluid properties are identified by the value of the local
Mach number M.

The most striking thing about figure 1(a) is the extraordinarily
small size of the region into which the large changes of flow around the
leading edge are concentrated. This is typified by the distance from the
stagnation point to the leading edge, along which the flow must accelerate
from M = 0 to M = 1. Even at the fairly large angle of attack of 13°,
this distance is only 0.0016 of the chord, which is too small to appear
in the present figure. In incompressible flow about a lifting flat plate
at the same angle of attack, the corresponding result as given by con-
formal transformation (see, e.g., ref. 9) is 0.05 of the chord. Obviously,
the stagnation point must move forward markedly as the free-stream Mach
number increases in the subsonic range. When Mach number 1 is reached,
it is, to the scale of the plate as a whole, practically coincident with
the edge. The representation of the leading-edge flow by a singularity
in which the stagnation point lies precisely at the edge is a well-known
approximation in thin-airfoil theory. The present results suggest that
the approximation should be even closer to the truth at transonic speeds
(as, for example, in the work of Guderley (ref. 1)) than it is in the
classical incompressible case.

As with the displacement of the stagnation point, the details of the
sonic line and limiting wave are not visible in figure 1(a). As nearly
as can be seen from this figure, the sonic line meets the leading edge
more or less directly from above, while the limiting wave comes into the
edge slightly from the rear. This appearance is, of course, at variance
with the qualitative description given earlier in connection with
sketch (a). If the results of figure 1(a) were all that were available,
however, one might be inclined to accept the statements of the present
paragraph as correct.

That the true state of affairs is quite different begins to appear
in figure 1(b). This figure shows the flow over the forward portion of
the plate to a scale 20 times that of figure 1(a). The present figure
also includes the separated streamline, which will be discussed later.

Enlargement to the scale of figure 1(b) is sufficient to show the
displacement of the stagnation point. A pronounced curvature of the sonic
line is also visible here, and this line seems now to meet the leading edge
from directly forward of the plate. The latter situation is, however,
still different from that described in connection with sketch (a). The
limiting wave in figure 1(b) appears to meet the edge from the rear, but
with greater slope and more curvature than were visible before.

To examine the situation at the leading edge in still greater detail, the results are replotted once more in figure 1(c), this time to a scale 200 times that of figure 1(a). Here at last it appears that the sonic line does indeed approach the leading edge from the underside of the plate. The manner in which the approach takes place, however, is still not clear.

To see the latter details, one is forced ultimately to a plot such as figure 1(d). This plot has a magnification 5000 times that of the original figure 1(a). Because of this very large magnification, the stagnation point in the present plot would lie approximately 50 inches off the page to the right. The trailing edge (whose position nevertheless determines the characteristic length in the problem) would be slightly more than 1/2 mile away. Despite the very large scale of figure 1(d), the results that appear here can be specified with good accuracy. This is because the hodograph transformation has the property of greatly enlarging the region near the leading edge relative to the rest of the field. Thus, a perfectly reasonable mesh interval for the finite-difference scheme in the hodograph plane (see part II) can provide sufficient data to define the lines of figure 1(d) without difficulty. To obtain comparable accuracy in calculations in the physical plane an impractically small interval would be required in the vicinity of the leading edge.

The contrast between the leading-edge flow as it appears in figure 1(d) and as it appeared originally in figure 1(a) is obvious. In figure 1(d) it can be seen that the sonic line does in fact meet the leading edge at right angles to the lower surface of the plate. (It can be shown that the curvature of the sonic line where it meets the plate is infinite.) The limiting wave in figure 1(d) comes into the edge from a direction slightly forward of the vertical. It thus approaches the plate much as the sonic line seemed to in the small plot of figure 1(a). To the present scale it is also possible to see something of the way in which the influence of the leading edge is propagated in the supersonic region. This is shown by the Mach lines included in the figure. The reader may find it interesting to compare these results with a similar plot of the Mach lines and streamlines in the classical Prandtl-Meyer flow (see, especially, p. 278 of ref. 10 and p. 171 of ref. 11).

Separated streamline.- The separated streamline is shown in figures 1(b) through 1(d) for the single case that has been calculated. In this case the pressure p_s on the separated streamline is given by $p_s/p_{t_\infty} = 0.000738$, where p_{t_∞} is the total pressure in the free stream. This is precisely the value of the pressure ratio that exists where the limiting wave meets the leading edge - that is, we have assumed that the flow remains attached to the leading edge until the limiting wave is reached and then immediately separates (see "Description of Flow Field"). The corresponding Mach number M_s on the separated streamline is 5.88, and the angle at which the streamline leaves the plate is 83-1/2° relative to the free-stream direction.

As can be seen from figure 1(b), the over-all dimensions of the
separated region are of the same order of magnitude as the distance from
the leading edge to the stagnation point. The length of limiting wave that
is needed to calculate the separated streamline is marked off in fig-
ure 1(b) by the point P. This is the point from which the downgoing
Mach wave to the reattachment point leaves the limiting wave. The angle
through which the flow must be deflected at the reattachment point turns
out to be 19°. This is well below the maximum deflection that can be
attained through an oblique shock wave in an inviscid flow at the assumed
Mach number of 5.88. Except for these observations, little can be said
about the separated flow until results become available for other values
of the pressure in the separated region.

Pressure Distribution

The distribution of pressure coefficient C_p on the lower surface
of the plate is shown in figure 2. Results for the complete surface are
given in figure 2(a) and for the region between the leading edge and stag-
nation point in figure 2(b). Included for comparison in figure 2(a) are
three additional sets of results obtained as follows:

(a) Directly from Guderley's small-disturbance analysis for $M_\infty = 1$
    (ref. 1),

(b) From Guderley's small-disturbance analysis with the approximate
    relationship between his hodograph variable η and the dimen-
    sionless speed w replaced by an exact relationship (see
    eq. (10a) of part II; this procedure was suggested and used by
    Guderley for a different problem in ref. 12),

(c) From the classical methods of conformal transformation for
    incompressible flow (see, e.g., ref. 9).

It can be seen from figure 2(a) that Guderley's work of reference 1
somewhat overestimates the pressure over the entire chord. The average
value of C_p given by his analysis is 0.59; that of the present work is
0.525. According to Guderley's calculations, the center of pressure is
at 35 percent of the chord; the present work puts it at 37.9. Considering
the fairly large angle of attack, however, the quantitative accuracy of
the small-disturbance analysis is remarkably good. The only major error
in the small-disturbance analysis occurs near the leading edge where the
approximate theory represents the stagnation point by an infinity at the
edge. The present results, by contrast, rise to the stagnation C_p of
1.275 very close to the edge and then drop to zero at the edge itself
(see fig. 2(b)). The effect of this qualitative difference on the inte-
grated force on the surface is obviously small.

According to figure 2(a), application of a correction to the small-
disturbance results as outlined in (b) above eliminates most of the

numerical error relative to the present findings. The discrepancies that
do remain are, for the most part, within the limits of accuracy to which
one can read numerical results from the graphs of reference 1. As regards
the leading-edge flow, the corrected curve gives a true stagnation value
of 1.275 but places the stagnation point still on the edge. For almost
all purposes, therefore, there appears to be no need to go beyond the
corrected small-disturbance analysis. Only if the details of the flow in
the immediate vicinity of the leading edge are of importance is it neces-
sary to resort to more accurate work.

The results for incompressible flow have been included in figure 2(a)
for general interest. They illustrate the relatively great displacement
of the stagnation point (C_p = 1.0) that occurs in the incompressible case.

CONCLUDING REMARKS

To what extent the results found here will apply to an actual airfoil
in a real fluid is an open question. The only experimental data bearing
on the problem are those of Wood (ref. 13), who made interferometric
studies of the flow at high subsonic speeds over a thin wedge at an angle
of attack of the lower surface of 11.5°. Wood's results for the lines of
constant Mach number (see, in particular, his figure 3(e) for M_∞ = 0.894)
show a distinct resemblance to the flow field of figure 1(a). Wood remarks
on the basis of his results that the stagnation point is "very close to
the leading edge," though precisely how close his measurements do not show.
At moderate distances above the leading edge, the sonic line found by Wood
looks reasonably like that of figure 1(a) if regard is had for differences
in free-stream Mach number. As to conditions in the immediate vicinity
of the edge, Wood takes his results to "indicate strongly that the sonic
line starts from the upper surface," though "refraction of the light in
the large density gradient . . . precludes following the contours all the
way to the surface." Because of the latter circumstance, the interfer-
ometer, in effect, views the field from essentially the scale of fig-
ure 1(a) (or, at best, something a slight bit larger). In view of the
minute size of the leading-edge flow as calculated in the present work,
Wood's inference must therefore be taken as tentative. As factors that
might move the sonic line from the lower surface, Wood cites the viscosity
of the fluid and the nonzero thickness of the real leading edge. Viscos-
ity will undoubtedly be of some influence, though the large negative
gradient of pressure near the leading edge would tend to minimize this
effect. (The pressure in the separated region will, of course, be fixed
by viscous phenomena, but these need not influence conditions on the lower
surface.) The thickness of the leading edge is likely to be of more
importance, since any real edge, though "sharp" in the ordinary sense,
will have an enormous thickness when viewed to the scale of figure 1(d).
It may well prove, however, that any changes from the theoretical pattern,
even from this latter source, are of only local effect and that the rela-
tively distant field will be correctly given by the theory. Certainly
there are many questions to be answered, and the remarks of this paragraph

are to be considered merely as miscellaneous thoughts on the subject. A
challenging field exists here for experimental research.

II - DETAILS OF ANALYSIS

An outline of the method of analysis has been given in part I of the
report. The material that follows is concerned with the mathematical
details. In the initial section the analytical basis is given for the
calculation of the mixed flow over the lower surface in the hodograph
plane. The main interest here is in the treatment of the free-stream
singularity. The second section is concerned with the numerical solution
of the hodograph problem. The procedures developed here, particularly as
regards the finite-difference equations in the supersonic region and near
the sonic line, may have application in other problems of mixed flow.
The third and final section deals briefly with the characteristics con-
struction used to find the purely supersonic flow over the separated region
on the upper surface.

ANALYTICAL BASIS FOR CALCULATION OF FLOW OVER LOWER SURFACE

Boundary-Value Problem in Hodograph Plane

. A representation of the flow over the lower surface of the plate in
the physical plane has been given in part I (see sketch (a)). The corre-
sponding picture in the hodograph plane is shown in sketch (b). The
variables here are the dimension-
less speed w (i.e., the ordinary
speed V made dimensionless
through division by the critical
speed a_*) and the flow inclination
θ (measured relative to the free-
stream direction). Corresponding
points in sketches (a) and (b) are
noted by the same symbols.

In the hodograph plane the
sonic speed appears as the circle
w = 1. The free stream appears
on this circle as the point O
located at θ = 0. All of the
streamlines issue from this
point, which is therefore sin-
gular. The lower surface of
the plate is represented by a
straight line passing through
the stagnation point C and
inclined at an angle of attack
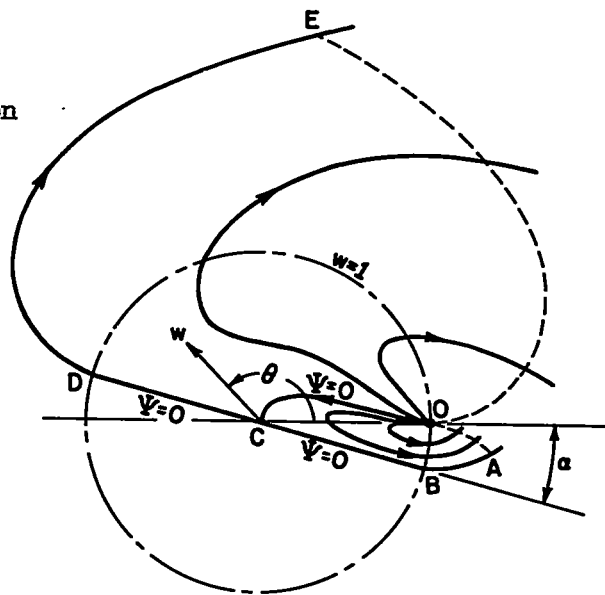
Sketch (b)

α to the free-stream direction. This line meets the sonic circle at points D and B, which correspond to the upstream side of the leading and trailing edges, respectively. The leading edge itself appears as the clockwise characteristic (i.e., epicycloid) through D; the trailing edge as the counterclockwise characteristic through B. The limiting Mach waves appear in the hodograph as the two characteristics passing through the free-stream point O. The point (E or A) at which each of these characteristics intersects the image of the corresponding edge fixes the extent of the edge that is of importance in determining the flow over the lower surface. The stagnation streamline runs in the hodograph from the free-stream point O to the stagnation point C, where it branches. The streamlines that lie above the stagnation streamline in the hodograph plane pass above the plate in the physical plane. Those that lie below this streamline pass below the plate.

To calculate the flow over the lower surface of the plate, a boundary-value problem must be solved in the region OABCDEO. If the stream function $\Psi(w,\theta)$ is taken as the dependent variable, the differential equation to be satisfied is the usual linear equation (see, e.g., ref. 14, p. 147)

$$w^2\Psi_{ww} + w\,\frac{1 - \dfrac{\gamma - 3}{\gamma + 1}\,w^2}{1 - \dfrac{\gamma - 1}{\gamma + 1}\,w^2}\,\Psi_w + \frac{1 - w^2}{1 - \dfrac{\gamma - 1}{\gamma + 1}\,w^2}\,\Psi_{\theta\theta} = 0 \tag{1}$$

where differentiation is indicated by the subscript notation. This equation is elliptic for $w < 1$ and hyperbolic for $w > 1$. The characteristics that exist for $w > 1$ are given by

$$d\theta = \pm\frac{1}{w}\left(\frac{w^2 - 1}{1 - \dfrac{\gamma - 1}{\gamma + 1}\,w^2}\right)^{1/2} dw \tag{2a}$$

or

$$\theta = \theta_{w=1} \pm \left[\left(\frac{\gamma + 1}{\gamma - 1}\right)^{1/2}\tan^{-1}\left(\frac{\gamma - 1}{\gamma + 1}\,\frac{w^2 - 1}{1 - \dfrac{\gamma - 1}{\gamma + 1}\,w^2}\right)^{1/2} - \tan^{-1}\left(\frac{w^2 - 1}{1 - \dfrac{\gamma - 1}{\gamma + 1}\,w^2}\right)^{1/2}\right] \tag{2b}$$

where $\theta_{w=1}$ is the value of θ at which the characteristic meets the sonic circle.

The boundary conditions to be satisfied in the problem are as follows:

1. The value of Ψ is constant - say 0 - on the boundary ABCDE.

2. The function Ψ has the proper singular behavior at the free-stream point O.

3. The streamline $\Psi = 0$ branches at the stagnation point C.

In order to represent the free stream, the singularity at O must have the following properties (cf. ref. 15):

(a) The function Ψ takes on all values from $+\infty$ to $-\infty$ at the point O.

(b) No singularities propagate along the limiting characteristics EO and AO. (This follows from the fact that no singularities exist in the boundary conditions at E and A.)

(c) The limiting characteristics transform into the finite part of the physical plane.

(d) The flow maps onto a single sheet in the physical plane.

Simple and useful expressions satisfying these requirements for the small-disturbance equivalent of equation (1) (i.e., the Tricomi equation) have been given by Guderley (refs. 1, 15, and 16) and Frankl (ref. 2). These expressions are the sum of two parts: (1) a doublet-like singularity antisymmetric in θ and (2) a vortex-like singularity symmetric in θ. Correspondingly simple expressions for the exact equation (1) have not been given, though Frankl (ref. 2) has obtained an infinite series of Chaplygin solutions that satisfies the given requirements. The present work will utilize the known singularities for the Tricomi equation (which predominate in any event) plus certain correction terms sufficient to account for a significant part of the difference between the approximate and exact results (see following section).

In view of boundary condition 1, boundary condition 3 can be met by requiring that

$$\Psi_w(0,\theta) = 0 \tag{3}$$

for any (and hence all) θ between $-\alpha$ and $\pi - \alpha$. To satisfy this condition in the present work we shall write Ψ in the form

$$\Psi = \Psi^a + C\Psi^s \tag{4}$$

where Ψ^a and Ψ^s are functions containing, respectively, the antisymmetric and symmetric parts of the free-stream singularity and C is a constant. The functions Ψ^a and Ψ^s will be required to satisfy individually the boundary condition 1 but not the boundary condition 3. The combined function Ψ will then constitute a solution of the complete problem - that is, will satisfy all the boundary conditions including 3 - provided C is evaluated such that

$$C = - \frac{\Psi_w{}^a(0,\theta)}{\Psi_w{}^s(0,\theta)}$$ (5)

The task now is to solve the individual boundary-value problems for Ψ^a and Ψ^s. In the end this will be done by numerical (i.e., finite-difference) means. First, however, certain analytical preliminaries are required, particularly with reference to the free-stream singularity.

Transformation of Differential Equation

To utilize the known singularities for the Tricomi equation, it is necessary to put equation (1) into a form closer to that of Tricomi. This can be done by a transformation of the type used by Guderley in the case of the equation for the Legendre potential (refs. 12 and 16):

$$\left.\begin{aligned} \eta &= \eta(w) \\[2mm] \psi &= \frac{1}{g(w)}\,\Psi \end{aligned}\right\}$$ (6)

Expressions for the functions η and g appearing here are found by substituting equations (6) into equation (1) and requiring that the resulting partial differential equation for ψ agree in its derivatives with the Tricomi equation - specifically, that it have the form

$$\psi_{\eta\eta} - \eta\psi_{\theta\theta} + b(\eta)\psi = 0$$ (7)

This procedure leads to the following ordinary differential equations for η and g:

$$\eta(\eta')^2 = \frac{1}{w^2}\left(\frac{w^2 - 1}{1 - \dfrac{\gamma - 1}{\gamma + 1}w^2}\right)$$ (8)

$$g' + \frac{1}{2}\left[\frac{\eta''}{\eta'} + \frac{1}{w}\left(\frac{1 - \frac{\gamma - 3}{\gamma + 1}w^2}{1 - \frac{\gamma - 1}{\gamma + 1}w^2}\right)\right]g = 0 \tag{9}$$

where the primes denote differentiation of a function with respect to its argument. By integration of equation (8), η is found as

$$\eta(w) = -\left\{\frac{3}{2}\left[\left(\frac{\gamma+1}{\gamma-1}\right)^{1/2}\tanh^{-1}\left(\frac{\gamma-1}{\gamma+1}\frac{1-w^2}{1-\frac{\gamma-1}{\gamma+1}w^2}\right)^{1/2} - \tanh^{-1}\left(\frac{1-w^2}{1-\frac{\gamma-1}{\gamma+1}w^2}\right)^{1/2}\right]\right\}^{2/3} \tag{10a}$$

for $w \leqq 1$ and

$$\eta(w) = \left\{\frac{3}{2}\left[\left(\frac{\gamma+1}{\gamma-1}\right)^{1/2}\tan^{-1}\left(\frac{\gamma-1}{\gamma+1}\frac{w^2-1}{1-\frac{\gamma-1}{\gamma+1}w^2}\right)^{1/2} - \tan^{-1}\left(\frac{w^2-1}{1-\frac{\gamma-1}{\gamma+1}w^2}\right)^{1/2}\right]\right\}^{2/3} \tag{10b}$$

for $w \geqq 1$. Here η has been taken equal to zero at $w = 1$ to satisfy the requirement that equation (7) change type at this point. (The similarity between equations (10b) and (2b) should be noted.) From equation (9), g is found as

$$g(w) = 2^{1/6}\left(\frac{\gamma+1}{2}\right)^{\frac{\gamma+2}{6(\gamma-1)}}\left(\frac{\eta}{w^2-1}\right)^{1/4}\left(1 - \frac{\gamma-1}{\gamma+1}w^2\right)^{\frac{\gamma+1}{4(\gamma-1)}} \tag{11}$$

where the constant of integration has been chosen (arbitrarily) to make $g = 1$ at $w = 1$. Plots of η and g as functions of w for $\gamma = 1.405$ are shown in figures 3 and 4, and tabular values are given in table I. The function η is positive at supersonic speeds ($w > 1$) and negative

at subsonic speeds ($w < 1$). It goes to negative infinity as $w \to 0$ and has a finite value (η_{max}) at the maximum speed $w_{max} = \sqrt{(\gamma + 1)/(\gamma - 1)}$. The function g goes to positive infinity as $w \to 0$ and to zero at w_{max}.

The function $b(\eta)$ in equation (7) is given implicitly by the equation

$$b(\eta) = \frac{1}{(\eta')^2} \left[\frac{g''}{g} + \frac{1}{w} \left(\frac{1 - \frac{\gamma - 3}{\gamma + 1} w^2}{1 - \frac{\gamma - 1}{\gamma + 1} w^2} \right) \frac{g'}{g} \right] \tag{12}$$

where g'/g and g''/g are to be evaluated with the aid of equations (9) and (8). A graph of b as a function of η is given in figure 5; tabular values are included in table I. The value of b is always negative; it approaches negative infinity as $\eta \to \eta_{max}$ and zero as $\eta \to -\infty$. For the subsequent work it is also necessary to know b as a power series in η about $\eta = 0$. The required expansion is

$$b(\eta) = b_0 + b_1\eta + b_2\eta^2 + \dots \tag{13}$$

where

$$b_0 = -0.9181$$

$$b_1 = -1.3164$$

$$b_2 = -1.0741$$
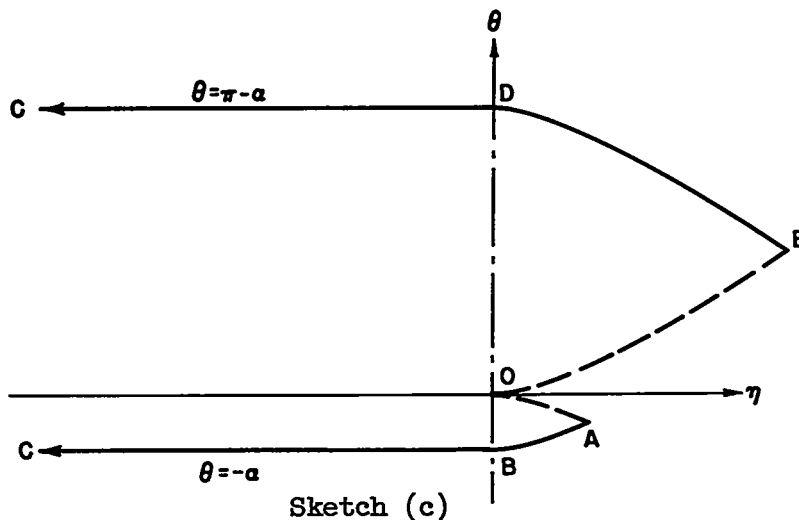
Sketch (c)

When transformed into the η,θ plane, the hodograph boundaries appear as shown in sketch (c). The characteristics of the differential equation (7), which define the boundaries for $\eta > 0$, are given by (see eqs. (2b) and (10b))

$$\theta = \theta_{\eta=0} \pm \frac{2}{3} \eta^{3/2} \qquad (14)$$

These are the same, of course, as for the Tricomi equation.

To carry out the solution for $\eta > 0$ we shall also require equation (7) in characteristic coordinates. These coordinates will be denoted here by r and l (corresponding to the right- and left-hand characteristics relative to the direction of positive η). They are defined by the equations

$$\theta = r - \frac{2}{3} \eta^{3/2} \qquad (15a)$$

$$\theta = l + \frac{2}{3} \eta^{3/2} \qquad (15b)$$

or equivalently

$$\eta = \left[\frac{3}{4} (r - l) \right]^{2/3} \qquad (16a)$$

$$\theta = \frac{r + l}{2} \qquad (16b)$$

When transformed into these coordinates, equation (7) becomes

$$[6(r - l)]^{2/3} \left[-\psi_{rl} + \frac{1}{6(r - l)} (\psi_r - \psi_l) \right] + b\psi = 0 \qquad (17)$$

Free-Stream Singularity

Method of treatment.- The finite-difference solution of problems involving a strong singularity (i.e., an infinity or discontinuity in the unknown or an infinity in its first derivatives) has been discussed by various writers (see, e.g., ref. 17). The usual procedure in linear problems is to write the dependent variable as the sum of two parts, each of which is individually a solution of the differential equation. The first part is a term of known analytical form containing the required singularity. The second part, free of singularity, is to be determined in accordance with the remaining, nonsingular boundary conditions. This part, being regular, can be found by numerical means. This procedure, unfortunately,

cannot be followed in the present case, since suitable analytical expressions for the singularity for the complete equation (7) are not known. Instead the procedure here will be to utilize the known singularities for the Tricomi equation plus certain analytical correction terms. These terms will reduce the order of the singularity in the remaining unknown to the point where it may safely be ignored in the numerical process.

The sonic singularities for the Tricomi equation - that is, for the equation

$$T(\psi) \equiv \psi_{\eta\eta} - \eta\psi_{\theta\theta} = 0 \tag{18}$$

have been discussed at length by Guderley in reference 16. Following Guderley's notation, we shall express these solutions in the form

$$\tilde{\psi} = |\eta|^n f_I(\zeta;n) \tag{19}$$

where ζ is a new variable defined by

$$\zeta \equiv \frac{9\theta^2}{4\eta^3} \tag{20}$$

The function f_I is a solution of a hypergeometric equation whose coefficients involve n as a parameter. Expressions for f_I are listed in reference 16 in terms of hypergeometric functions. As shown in reference 16, the values of n required to represent a uniform free stream are -5/2 for the antisymmetric singularity and -1 for the symmetric singularity.

To utilize the solutions (19) in the present case, we begin by rewriting equation (7) as

$$T(\psi) = - (b_0 + b_1\eta + b_2\eta^2 + \ldots)\psi \tag{21}$$

For reasons that will appear directly, the solution of the boundary-value problem (for either ψ^a or ψ^s) is then taken in the form

$$\psi = A\left(\tilde{\psi} + \sum_{i=0}^{m} \hat{\psi}_i\right) + \chi \tag{22}$$

where A is any convenient constant. The $\hat{\psi}_i$ that appear here are

singular correction functions[2] of the form $\hat{\psi}_i = |\eta|^{n_i} g_i(\zeta)$ and X is added to satisfy the nonsingular boundary conditions. In contrast to the usual procedure outlined above, none of the terms in equation (22) are individually solutions of the differential equation (21). To make clear the reasons for the foregoing choice - and at the same time derive equations for $\hat{\psi}$ and X - we substitute equation (22) into equation (21) and arrange the result according to the following scheme:

$$
\left.
\begin{aligned}
\frac{1}{A}\,[T(X) + bX]\\
+\ T(\hat{\psi}_0)\\
+\ T(\hat{\psi}_1)\\
+\ T(\hat{\psi}_2)\\
+\ T(\hat{\psi}_3)\\
+\ \ldots\\
+\ T(\hat{\psi}_m)
\end{aligned}
\right\}
= -
\left\{
\begin{aligned}
&b_0\tilde{\psi}\\
&+ b_1\eta\tilde{\psi}\\
&+ b_2\eta^2\tilde{\psi} && + b_0\hat{\psi}_0\\
&+ b_3\eta^3\tilde{\psi} && + b_1\eta\hat{\psi}_0 && + b_0\hat{\psi}_1\\
&+ \ldots \ldots \ldots \ldots \ldots \ldots\\
&+ b_m\eta^m\tilde{\psi} && + b_{m-2}\eta^{m-2}\hat{\psi}_0 + b_{m-3}\eta^{m-3}\hat{\psi}_1 + \ldots + b_0\hat{\psi}_{m-2}\\
&+ b_{m+1}\eta^{m+1}\tilde{\psi} + b_{m-1}\eta^{m-1}\hat{\psi}_0 + b_{m-2}\eta^{m-2}\hat{\psi}_1 + \ldots + b_1\eta\hat{\psi}_{m-2} + b_0\hat{\psi}_{m-1}\\
&+ b_{m+2}\eta^{m+2}\tilde{\psi} + b_m\eta^m\hat{\psi}_0 \quad + b_{m-1}\eta^{m-1}\hat{\psi}_1 + \ldots + b_2\eta^2\hat{\psi}_{m-2} + b_1\eta\hat{\psi}_{m-1} + b_0\hat{\psi}_m\\
&+ \ldots \ldots \ldots \ldots \ldots \ldots \ldots \ldots \ldots \ldots \ldots \ldots \ldots
\end{aligned}
\right.
$$

$$(23)$$

The idea here is that we determine $\hat{\psi}_0$, $\hat{\psi}_1$, etc., such that $T(\hat{\psi}_0) = -b_0\tilde{\psi}$, $T(\hat{\psi}_1) = -b_1\eta\tilde{\psi}$, etc. Since, in general, $T(\hat{\psi}_i) = |\eta|^{n_i-2} h_i(\zeta)$ if $\hat{\psi}_i = |\eta|^{n_i} g_i(\zeta)$, and since we have $\tilde{\psi} = |\eta|^n f_I$, it follows that the correction functions must proceed like $\hat{\psi}_0 = |\eta|^{n+2} g_0$, $\hat{\psi}_1 = |\eta|^{n+3} g_1$, etc. The scheme of equation (21) follows accordingly. (Note in particular that for $i \geq 2$ the previous correction functions must be included together with $\tilde{\psi}$ on the right-hand side of the equation.) It thus appears that the expression (22) will constitute a solution of the differential equation (21), provided the general correction $\hat{\psi}_i$ and the function X satisfy the following nonhomogeneous differential equations:

---

[2]Correction functions of this type have also been used by Frankl in reference 2.

$$T(\widehat{\psi}_i) = - (b_i\eta^i\widetilde{\psi} \quad + b_{i-2}\eta^{i-2}\widehat{\psi}_0 + b_{i-3}\eta^{i-3}\widehat{\psi}_1 + \ldots + b_0\widehat{\psi}_{i-2})$$

$$\tag{24}$$

for $i = 0, 1, \ldots, m$ and

$$
\begin{aligned}
T(X) + bX = - A[&(b_{m+1}\eta^{m+1} + b_{m+2}\eta^{m+2} \quad + \ldots)\widetilde{\psi} \\
&+ (b_{m-1}\eta^{m-1} + b_m\eta^m \quad + \ldots)\widehat{\psi}_0 \\
&+ (b_{m-2}\eta^{m-2} + b_{m-1}\eta^{m-1} \quad + \ldots)\widehat{\psi}_1 \\
&+ \ldots \ldots \ldots \ldots \ldots \ldots \\
&+ (b_0 \quad\quad + b_1\eta \quad\quad + \ldots)\widehat{\psi}_{m-1} \\
&+ (b_0 \quad\quad + b_1\eta \quad\quad + \ldots)\widehat{\psi}_m]
\end{aligned}
$$

$$\tag{25}$$

It is apparent that the correction functions $\widehat{\psi}_i$, like the original function $\widetilde{\psi}$, are singular at the origin. The singularity, however, becomes weaker (i.e., makes its first appearance in progressively higher-order derivatives) as i increases. The function X is also singular at the origin, the singularity here being one order weaker than that in $\widehat{\psi}_m$.

Equations (24) and (25) form the basis for the present work. As will be seen, equation (24) can be solved analytically for as large a value of i as will be required. Solution for arbitrary i would be very difficult. (This is the reason for not taking $m = \infty$ and thus reducing X to a regular function.) Equation (25) will be solved numerically, subject to appropriate boundary conditions, by ignoring the singularity in X at the origin and applying the finite-difference techniques ordinarily used for a regular function. If the singularity is sufficiently weak, the resulting error in the over-all solution should be small. To make a numerical solution possible at all, a minimum requirement is that the right-hand side of equation (25) must be finite and single-valued at the origin. Since $\widetilde{\psi} = |\eta|^n f_I$, it can be seen that for this requirement to be satisfied we must choose m such that $m+1+n > 0$ or that $m > -(n + 1)$. For the antisymmetric singularity ($n = -5/2$) we shall therefore take $m = 2$. For the symmetric singularity ($n = -1$), m will be taken equal to 1. In the antisymmetric case the singularity that then remains in X first appears in the derivative $X_{\theta\theta}$ (but not in $X_{\eta\eta}$ or $X_{\eta\theta}$). In the symmetric case it first appears in the third-order derivatives. Ignoring singularities of this order in the solution for X may be expected to cause negligible error, especially in the vicinity of the plate.

Solution for correction functions.- According to the foregoing, expressions for the correction functions $\widehat{\psi}_i$ are needed for $i = 0, 1, 2.$

These are found by solving equation (24), which can also be written

$$\hat{\Psi}_{i_{\eta\eta}} - \eta\hat{\Psi}_{i_{\theta\theta}} = - b_i\eta^i\tilde{\Psi} + \sum_{t=0}^{i-2} b_{i-2-t}\eta^{i-2-t}\hat{\Psi}_t \qquad (26)$$

To carry out the solution we introduce a function $\overline{\Psi}$ that satisfies the Tricomi equation

$$\overline{\Psi}_{\eta\eta} - \eta\overline{\Psi}_{\theta\theta} = 0 \qquad (27)$$

and has the property that

$$\overline{\Psi}_{\theta\theta} = \tilde{\Psi} \qquad (28)$$

(Expressions for $\overline{\Psi}$ will be given later.)[3] From equations (27) and (28) we also have the relations

$$\overline{\Psi}_{\eta\eta} = \eta\overline{\Psi}_{\theta\theta} = \eta\tilde{\Psi} \qquad (29a)$$

and

$$\overline{\Psi}_{\eta\theta\theta} = \overline{\Psi}_{\theta\theta\eta} = \tilde{\Psi}_{\eta} \qquad (29b)$$

The solution of equation (26) will now be assumed in the form

$$\hat{\Psi}_i = p_i\eta^{i-1}\overline{\Psi} + q_i\eta^i\overline{\Psi}_{\eta} \qquad (30)$$

where p_i and q_i are constants whose values are to be found. By differentiating this expression and making use of relations (29), one obtains

---

[3]This approach was suggested by Gottfried Guderley, to whom the authors are much indebted.

$$\hat{\psi}_{i_{\eta\eta}} = p_i[(i-1)(i-2)\eta^{i-3}\overline{\psi} + 2(i-1)\eta^{i-2}\overline{\psi}_\eta + \eta^{i-1}\overline{\psi}_{\eta\eta}] +$$

$$q_i[i(i-1)\eta^{i-2}\overline{\psi}_\eta + (2i+1)\eta^i\tilde{\psi} + \eta^{i+1}\tilde{\psi}_\eta] \qquad (31a)$$

$$\hat{\psi}_{i_{\theta\theta}} = p_i\eta^{i-1}\overline{\psi}_{\theta\theta} + q_i\eta^i\tilde{\psi}_\eta \qquad (31b)$$

Substitution of expressions (31) and (30) into equation (26) then gives, in view of equation (27),

$$q_i(2i+1)\eta^i\tilde{\psi} + p_i(i-1)(i-2)\eta^{i-3}\overline{\psi} + (2p_i + iq_i)(i-1)\eta^{i-2}\overline{\psi}_\eta$$

$$= -b_i\eta^i\tilde{\psi} - \eta^{i-3}\overline{\psi}\sum_{t=0}^{i-2}b_{i-2-t}p_t - \eta^{i-2}\overline{\psi}_\eta\sum_{t=0}^{i-2}b_{i-2-t}q_i$$

For this equation to be satisfied for all η we must have

$$\left. \begin{array}{l} q_i(2i+1) = -b_i \\[3ex] p_i(i-1)(i-2) = -\displaystyle\sum_{t=0}^{i-2}b_{i-2-t}p_t \\[3ex] (2p_i + iq_i)(i-1) = -\displaystyle\sum_{t=0}^{i-2}b_{i-2-t}q_i \end{array} \right\} \qquad (32)$$

These are three equations for the two unknowns p_i and q_i, so that in general a solution cannot be found. For $i = 0, 1, 2$, however, certain of the equations either coincide or disappear, and a solution can be obtained as follows:

For $i = 0$ equations (32) reduce to

$$q_0 = -b_0$$

$$-2p_0 = 0$$

$$-2p_0 = 0$$

which have the solution $p_0 = 0$, $q_0 = -b_0$.

For $i = 1$ equations (32) become

$$3q_1 = -b_1$$

$$p_1 \cdot 0 = 0$$

$$(2p_1 + q_1) \cdot 0 = 0$$

We thus have p_1 arbitrary - say 0 - and $q_1 = -b_1/3$.[4]

For $i = 2$ equations (32) become

$$5q_2 = -b_2$$

$$p_2 \cdot 0 = -b_0 p_0$$

$$2p_2 + 2q_2 = -b_0 q_0$$

Since $p_0 = 0$ and $q_0 = -b_0$, these have the solution $q_2 = -b_2/5$ and $p_2 = (b_0^2/2) + (b_2/5)$.

By using these results in equation (30), we thus obtain the required correction functions as

$$
\left.
\begin{aligned}
\hat{\psi}_0 &= -b_0 \overline{\psi}_\eta \\[2mm]
\hat{\psi}_1 &= -\frac{b_1}{3}\, \eta \overline{\psi}_\eta \\[2mm]
\hat{\psi}_2 &= \left(\frac{b_0^2}{2} + \frac{b_2}{5}\right) \eta \overline{\psi} - \frac{b_2}{5}\, \eta^2 \overline{\psi}_\eta
\end{aligned}
\right\} \tag{33}
$$

[4]It is to be expected that p_1 would be arbitrary, since for $i = 1$ the first term of expression (27) reduces to $p_1 \overline{\psi}$, and this term will, by virtue of equation (24), disappear when substituted into the left-hand side of equation (23), irrespective of the value of p_1.

If it were required, a solution for $\hat{\psi}_3$ could be found by taking a suitable value of $p_1 \neq 0$. A solution for $\hat{\psi}_4$ (and higher) in the form of equation (27) is apparently impossible.

To apply equations (33) it remains to write expressions for $\bar{\psi}$ and $\bar{\psi}_\eta$. With the aid of the equations of reference 16 (pp. 58 and 34-35) it can be shown that, if $\psi = |\eta|^n f_I(\zeta;n)$ as given by equation (19), then an expression for $\bar{\psi}$ that satisfies equations (27) and (28) is

$$\bar{\psi} = K|\eta|^{n+3} f_I(\zeta;n + 3) \tag{34}$$

where

$$K = \frac{(4n + 1)(4n + 7)}{(n + 2)(n + 3)(2n + 1)(2n + 3)}$$

By differentiating equation (34) and having recourse again to the equations of reference 16, it can also be shown that

$$\bar{\psi}_\eta = K|\eta|^{n+2}(\text{sign } \eta)\left[(n+3)f_I(\zeta;n+3) - \frac{2(n+2)(n+3)}{4n+7}|\zeta|^{1/2}(\text{sign } \theta)f_I\left(\zeta;n+\frac{3}{2}\right)\right] \tag{35}$$

where (sign η) or (sign θ) are quantities with absolute value 1 and the sign of η or θ.

Final relations.- By using equations (19), (33), (34), and (35) in conjunction with equations (22) and (25), we can now write the final relations to be used in solving the boundary-value problems for ψ^a and ψ^s.

Problem for ψ^a: In this case the solution must contain the anti-symmetric singularity, in which case $n = -5/2$ and $m = 2$. Equation (22), written for ψ^a, thus becomes, after substitution from equations (33),

$$\psi^a = A^a\left[\bar{\psi}^a + \left(\frac{b_0^2}{2} + \frac{b_2}{5}\right)\eta\bar{\psi}^a - \left(b_0 + \frac{b_1}{3}\eta + \frac{b_2}{5}\eta^2\right)\bar{\psi}_\eta^a\right] + \chi^a \tag{36}$$

The differential equation for the unknown X^a is found by substituting equations (33) into equation (25) and can be written

$$X^a_{\eta\eta} - \eta X^a_{\theta\theta} + bX^a = -A^a\left\{[b - (b_0 + b_1\eta + b_2\eta^2)]\tilde{\psi}^a + b\left(\frac{b_0^2}{2} + \frac{b_2}{5}\right)\eta\bar{\psi}^a - \left[b\left(b_0 + \frac{b_1}{3}\eta + \frac{b_2}{5}\eta^2\right) - b_0^2\right]\bar{\psi}^a_\eta\right\}$$

(37)

The formulas to be used in computing $\tilde{\psi}^a$, $\bar{\psi}^a$, and $\bar{\psi}^a_\eta$, as obtained from equations (19), (34), and (35), are

$$\left.\begin{aligned}
\tilde{\psi}^a &= |\eta|^{-5/2}f_I\left(\zeta;\ -\frac{5}{2}\right) \\[2ex]
\bar{\psi}^a &= -\frac{27}{2}|\eta|^{1/2}f_I\left(\zeta;\ \frac{1}{2}\right) \\[2ex]
\bar{\psi}^a_\eta &= -\frac{27}{4}|\eta|^{-1/2}(\text{sign }\eta)\left[f_I\left(\zeta;\ \frac{1}{2}\right) - \frac{1}{3}|\zeta|^{1/2}(\text{sign }\theta)f_I(\zeta;\ -1)\right]
\end{aligned}\right\}$$

(38)

These quantities are all antisymmetric with respect to θ, so that computations need be carried through only for positive θ.

Problem for ψ^s: Here the solution contains the symmetric singularity, in which case $n = -1$ and $m = 1$. The equation for ψ^s is therefore

$$\psi^s = A^s\left[\tilde{\psi}^s - \left(b_0 + \frac{b_1}{3}\eta\right)\bar{\psi}^s_\eta\right] + X^s$$

(39)

and the differential equation for X^s is

$$X^s_{\eta\eta} - \eta X^s_{\theta\theta} + bX^s = -A^s\left\{[b - (b_0 + b_1\eta)]\tilde{\psi}^s - b\left(b_0 + \frac{b_1}{3}\eta\right)\bar{\psi}^s_\eta\right\}$$

(40)

The formulas for $\tilde{\psi}^s$ and $\tilde{\psi}_\eta^s$ are

$$
\left.
\begin{aligned}
\tilde{\psi}^s &= |\eta|^{-1} f_I(\zeta;\,-1) \\[2ex]
\tilde{\psi}_\eta^s &= \eta\left[9 f_I(\zeta;2) - 6|\zeta|^{1/2}(\text{sign }\theta) f_I\left(\zeta;\,\tfrac{1}{2}\right)\right]
\end{aligned}
\right\}
\tag{41}
$$

These quantities are both symmetric with respect to θ.

Formulas for the $f_I(\zeta;n)$ that appear in equations (38) and (41) are given by Guderley in reference 16 in terms of hypergeometric series. For the values of n required here, however, the results can be put in closed form analogous to that given by Frankl for $n = -5/2$ in reference 2. If a new variable s is introduced according to the definition

$$
s \equiv \frac{\theta}{\sqrt{\theta^2 - \dfrac{4}{9}\eta^3}} = \sqrt{\frac{\zeta}{\zeta - 1}}
\tag{42}
$$

the pertinent formulas are

$$
\left.
\begin{aligned}
f_I\left(\zeta;\,-\tfrac{5}{2}\right) &= \frac{81}{16}\,|s^2 - 1|^{\frac{5}{6}}\left[\left(\tfrac{1}{3} + s\right)(1 - s)^{\frac{1}{3}} - \left(\tfrac{1}{3} - s\right)(1 + s)^{\frac{1}{3}}\right] \\[2ex]
f_I(\zeta;\,-1) &= \frac{3}{2}\,|s^2 - 1|^{\frac{1}{3}}\left[(1 - s)^{\frac{1}{3}} + (1 + s)^{\frac{1}{3}}\right] \\[2ex]
f_I\left(\zeta;\,\tfrac{1}{2}\right) &= -\frac{1}{2}\,|s^2 - 1|^{-\frac{1}{6}}\left[(1 - s)^{\frac{1}{3}} - (1 + s)^{\frac{1}{3}}\right] \\[2ex]
f_I(\zeta;2) &= -\frac{1}{2}\,|s^2 - 1|^{-\frac{2}{3}}\left[\left(\tfrac{1}{3} + s\right)(1 - s)^{\frac{1}{3}} + \left(\tfrac{1}{3} - s\right)(1 + s)^{\frac{1}{3}}\right]
\end{aligned}
\right\}
\tag{43}
$$

Equations for Transformation to Physical Plane

After the boundary-value problems for ψ^a and ψ^s are solved, Ψ is found from equations (6) and (4), and the solution is transformed to the physical plane. If x and y form a right-hand coordinate system with x in the free-stream direction, the transformation equations can be put in the form (cf. ref. 14, pp. 146-147)

$$\left.\begin{aligned}dx &= x_w dw + x_\theta d\theta \\ dy &= y_w dw + y_\theta d\theta\end{aligned}\right\} \tag{44}$$

where

$$\left.\begin{aligned}x_w &= -\frac{\rho_t}{\rho w a_*}\left[\sin\theta\,\Psi_w + \frac{1-w^2}{1-\dfrac{\gamma-1}{\gamma+1}w^2}\cos\theta\,\frac{\Psi_\theta}{w}\right]\\[2ex]x_\theta &= \frac{\rho_t}{\rho w a_*}\left[w\cos\theta\,\Psi_w - \sin\theta\,\Psi_\theta\right]\\[2ex]y_w &= \frac{\rho_t}{\rho w a_*}\left[\cos\theta\,\Psi_w - \frac{1-w^2}{1-\dfrac{\gamma-1}{\gamma+1}w^2}\sin\theta\,\frac{\Psi_\theta}{w}\right]\\[2ex]y_\theta &= \frac{\rho_t}{\rho w a_*}\left[w\sin\theta\,\Psi_w + \cos\theta\,\Psi_\theta\right]\end{aligned}\right\} \tag{45}$$

and

$$\frac{\rho_t}{\rho} = \left(1 - \frac{\gamma-1}{\gamma+1}w^2\right)^{-\frac{1}{\gamma-1}} \tag{46}$$

In the present work all distances will be made dimensionless in terms of the airfoil chord, which can be written

$$c = \frac{x_B - x_D}{\cos\alpha}$$

where x_D and x_B are the x coordinates of the leading and trailing edges (measured relative to any convenient origin). By applying equations (44) through (46) along the line DCB, for which $d\theta = 0$ (see sketch (b)), one can write

$$x_B - x_D = \int_D^B x_w dw = \frac{\cos \alpha}{a_*} I \tag{48}$$

where

$$I \equiv - \int_D^B \frac{1 - w^2}{\left(1 - \frac{\gamma-1}{\gamma+1} w^2\right)^{\frac{\gamma}{\gamma-1}}} \frac{\Psi_\theta}{w^2} d(\pm w) \tag{49}$$

It is understood from the limits that the integration is taken from D to B along the image of the plate. The minus sign in the differential $d(\pm w)$ is to be used from D to C and the plus sign from C to B. Combination of equations (47) and (48) then gives

$$c = \frac{1}{a_*} I \tag{50}$$

from which we can write

$$\left. \begin{aligned} d\left(\frac{x}{c}\right) &= \frac{1}{I} \left(a_* x_w dw + a_* x_\theta d\theta\right) \\[2mm] d\left(\frac{y}{c}\right) &= \frac{1}{I} \left(a_* y_w dw + a_* y_\theta d\theta\right) \end{aligned} \right\} \tag{51}$$

Equations (51), (49), and (45) are the basis for the numerical transformation from the hodograph plane to the physical plane.

To transform the characteristic lines in the supersonic region, it is convenient to rewrite the transformation equations in the coordinates r and l. This can be done on the basis of equations (15) and (8). The results are

$$d\left(\frac{x}{c}\right) = \frac{1}{I}\left(a_*x_r dr + a_*x_l dl\right)$$

$$d\left(\frac{y}{c}\right) = \frac{1}{I}\left(a_*y_r dr + a_*y_l dl\right) \Bigg\}$$

(52)

where

$$x_r = \frac{\rho_t}{\rho w a_*}\left(\beta \cos \theta - \sin \theta\right)\Psi_r$$

$$x_l = -\frac{\rho_t}{\rho w a_*}\left(\beta \cos \theta + \sin \theta\right)\Psi_l$$

$$y_r = \frac{\rho_t}{\rho w a_*}\left(\beta \sin \theta + \cos \theta\right)\Psi_r$$

$$y_l = -\frac{\rho_t}{\rho w a_*}\left(\beta \sin \theta - \cos \theta\right)\Psi_l$$

(53)

and

$$\beta = \left(\frac{w^2 - 1}{1 - \dfrac{\gamma - 1}{\gamma + 1}w^2}\right)^{1/2}$$

NUMERICAL SOLUTION FOR FLOW OVER LOWER SURFACE

General Scheme

The numerical solution of the boundary-value problems for ψ^a and ψ^s will be based on equations (36), (37) and (39), (40). To explain the general scheme, it is convenient to introduce the linear differential operator $L_\partial(F)$ defined equivalently by

$$L_{\partial}(F) \equiv \begin{cases} F_{\eta\eta} - \eta F_{\theta\theta} + bF & \text{(54a)} \\[2em] [6(r-\imath)]^{2/3}\left[-F_{r\imath} + \dfrac{1}{6(r-\imath)}(F_r - F_\imath)\right] + bF & \text{(54b)} \end{cases}$$

In this notation the differential equations (7) and (17) become

$$L_{\partial}(\psi) = 0 \tag{55}$$

It is also convenient for present purposes to write the solutions (36) and (39) in the form

$$\psi = AM + X \tag{56}$$

where M is a shorthand notation for the quantity appearing in brackets in the earlier representations. By substituting this expression into equation (55), we can then write the differential equations (37) and (40) in the form

$$L_{\partial}(X) = -AL_{\partial}(M) \tag{57}$$

where $L_{\partial}(M)$ is identical to the quantity in braces on the right-hand side of the earlier equations.

To carry out a solution for the unknown X, we begin in the usual fashion by replacing the differential expression on the left-hand side of equation (57) by a corresponding difference expression. This is done as usual by covering the region of solution with a suitable mesh and approximating the differential operator $L_{\partial}(F)$ by an appropriate difference operator at each mesh point. This difference operator, denoted by $L_{\triangle}(F)$, will appear in the form

$$L_{\triangle}(F) = L_{\triangle}(F_0, F_1, \ldots, F_n)$$

where the F_j (j = 0, 1, . . . , n) denote the values of F at the point in question and at n adjacent points. In this manner the differential equation (57) is replaced at each mesh point by a difference equation of the type

$$L_\triangle(X) = -AL_\partial(M) \tag{58}$$

So far the procedure is conventional. At this point one could proceed, also in conventional fashion, to solve the difference equation (58) for X. The required values of X on the boundary would follow directly from equation (56) and the known condition that $\psi = 0$ on the boundary. Following the determination of X at all mesh points, the corresponding values of ψ would then be calculated, again by means of equation (56).

Considerable simplification over the foregoing method can be obtained, however, by using a method due to Woods (ref. 17). According to this method, instead of solving for X, one uses equation (56) immediately to replace X_j for all mesh points in equation (58) by the equivalent $\psi_j - AM_j$. (The special case of equations involving the origin, at which $M_j = \infty$, will be treated later.) In this manner one obtains a system of difference equations of the form

$$L_\triangle(\psi) = -A[L_\partial(M) - L_\triangle(M)] \tag{59}$$

This system can be solved directly for ψ. This method, though completely equivalent mathematically to that outlined in the preceding paragraph, has a great advantage for the present work. This stems from the fact that the right-hand side of equation (59), which is proportional to the difference between L_∂ and $L_\triangle$ both operating on M, tends to zero as the distance from the origin increases. At some distance (depending upon the value of A, the size of the mesh interval, and the accuracy desired in the work) the right-hand side will, in fact, become negligible. Beyond this distance equation (59) reduces for all practical purposes to

$$L_\triangle(\psi) = 0 \tag{60}$$

(which is the same as would have been obtained if the finite-difference approximation had been introduced into equation (55)). This means that the values of $L_\partial(M)$ and M need be calculated at only a small percentage of the mesh points, instead of at all points as would be the case if the method based on equation (58) were used. Furthermore, the advantages to the computer of working with the familiar variable ψ, with boundary conditions directly in this variable, are considerable.

The foregoing procedure must be modified when one of the X_j in the difference equation (58) - say X_k - is located at the origin. This situation will prevail in the difference equations at the origin itself and at points adjacent thereto. In these equations X_k cannot be replaced by $\psi_k - AM_k$ since M_k is infinite. It must therefore remain in the equation, although the other X_j can be replaced as before. Even in such cases, however, the general procedure can be formally retained if we look

upon X_k as a fictitious value of ψ - say ψ_k - and take M_k as arbi-
trarily zero. If this convention is used in the expressions to be given
below for $L_\Delta(F)$, equation (59) will automatically provide the correct
difference equations at the origin and adjacent points. The value of ψ_k
that is computed, however, will have no real significance.

Details of Finite-Difference Equations

To apply equation (59), it is necessary to obtain expressions for
the difference operator $L_\Delta(F)$. This will be done differently in three
different regions of the hodograph, as illustrated schematically in
sketch (d). (Here only positive θ will be discussed. The procedures
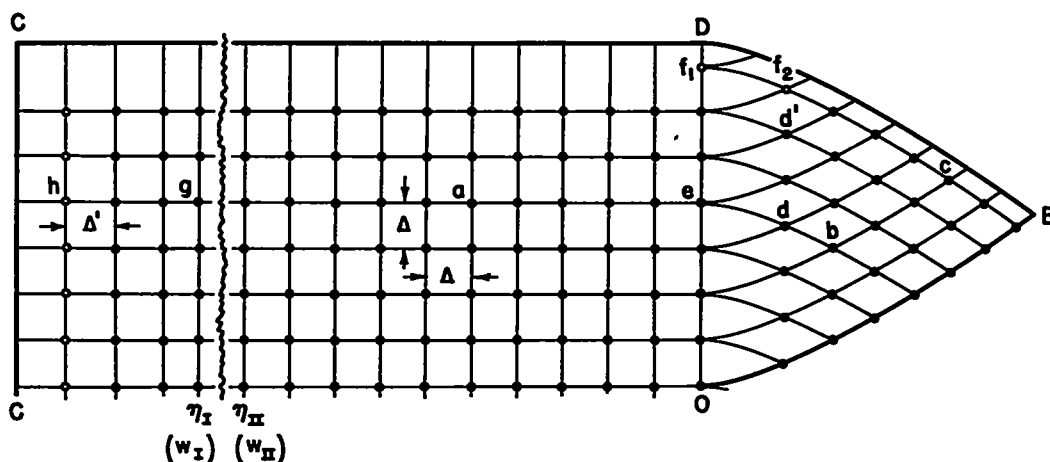
Sketch (d)

for negative θ will be obvious.) For purposes of the present discussion
η_I is used to denote some convenient negative multiple of Δ, where Δ
is the interval of the finite-difference mesh in the η,θ variables; η_{II}
is defined according to the relation $\eta_{II} = \eta_I + \Delta$. With this notation,
the three regions in the hodograph and the procedures used in each are
briefly as follows (details will be given later):

$\eta_I < \eta \leqq 0$: In this region the field is covered with a square mesh
of basic interval Δ in the η and θ directions. Adjacent to the upper
boundary the interval is adjusted (made greater than Δ) so that the
terminal mesh points lie on the boundary. Throughout the region the dif-
ference operator is found by approximation to the differential operator
in the form given by equation (54a).

$\eta > 0$: In this region the mesh is formed by lines of constant
r and l as shown in the sketch (see also eqs. (15)). It is convenient
here to include a line of constant r beginning on the sonic line a dis-
tance Δ above the uppermost line in the subsonic field. At all points

(except those next to the sonic line) the difference operator is obtained
by approximating the differential operator in the form given by
equation (54b).[5]

$\eta < \eta_{II}$: Here a reversion is made from η to the original vari-
able w. This is done to avoid difficulties arising from the fact that η
extends to $-\infty$. A rectangular mesh is employed with basic interval Δ in
the θ direction and Δ' in the w direction. At the right-hand side
of the region the intervals in w are adjusted so that vertical mesh
lines fall at locations w_I and w_{II} corresponding to η_I and η_{II}. At
all points the finite-difference equations are based not on equation (59)
but on the differential equation (1) for Ψ. For this to be permissible,
η_I must be taken far enough to the left that equation (59), if used,
would have reduced computationally to the homogeneous equation (60).

With the procedures just outlined, the mesh points fall into eight
categories, each of which requires a different treatment. These categories
are listed as follows (a typical point in each category is indicated by a
corresponding letter in sketch (d)):

    a. Subsonic points in η,θ coordinates
    b. Regular supersonic points
    c. Supersonic points next to corner characteristic
    d. Supersonic points next to sonic line
    e. Points on sonic line
    f. Points near intersection of sonic line and corner characteristic
    g. Regular subsonic points in w,θ coordinates
    h. Points next to stagnation point

In most categories the finite-difference approximation will be obtained
by some variation of the usual series-expansion procedure. In this proce-
dure the function F at each of a number of mesh points adjacent to the
given point is expanded in terms of a truncated Taylor's series about the
given point. These series can be regarded as simultaneous equations for
the derivatives of F at the given point and solved accordingly. Follow-
ing this approach, we obtain expressions for the derivatives in terms of
the local dimensions of the mesh and the values of F at the points

---

[5]In the earlier work of references 3 and 4, attempts to devise a
numerical procedure in the supersonic region, using either rectangular or
characteristic coordinates, were not successful. In these reports, which
employed the Tricomi approximation, the difficulty was overcome by elimi-
nating this region and substituting an integral relation as a boundary
condition on the sonic line. For the present work it has been found pos-
sible to set up a successful numerical procedure by having proper regard
(which was not done previously) for the region of dependence of each point
in the characteristics mesh. This was essential here, since an integral
relation like that used before is not available for the exact equation.
Even if it were, however, the present method would probably be preferred
from the computational point of view.

considered. By substituting these results into the pertinent differential
relations, the required finite-difference approximations are obtained.
The number of terms retained in the Taylor's series in any given case, as
well as the number of adjacent points utilized, will depend upon the order
of the derivatives to be approximated, the local arrangement of the mesh,
and the degree of accuracy desired. The policy here will be to use the
simplest expressions possible consistent with the analytical and geometri-
cal situation at the point in question. The requisite accuracy will then
be obtained by reduction of the mesh interval to whatever degree appears
needed in various parts of the field. The details of the derivation will
be given only when the procedure differs from that ordinarily encountered.
(For detailed examples of the ordinary kind, see ref. 3.)

Subsonic points in η,θ coordinates.- The situation at points of
this kind is shown in sketch (e). For application next to the upper and
lower boundaries, irregular mesh intervals are
provided in the vertical direction. These are of
length h and k relative to the basic interval
Δ. By straightforward application of the series-
expansion procedure to the approximation of the
differential operator (54a), one obtains for the
difference operator at 0
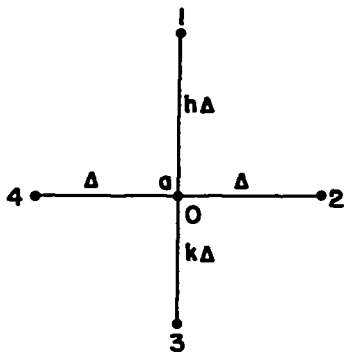
$$L_\Delta(F) = \frac{2}{\Delta^2}\left[\frac{F_2+F_4}{2} - \eta_0\frac{kF_1+hF_2}{hk(h+k)} - \left(1-\frac{\eta_0}{hk}\right)F_0\right]+b_0F_0$$

Sketch (e)   (61)

where the subscripts 0, 1, 2, etc., denote values of F at the correspond-
ing points in the sketch. (The quantity b_0 that appears in this and
subsequent finite-difference expressions should not be confused with the
b_0 that was introduced previously in the treatment of the free-stream
singularity; cf. eqs. (21) through (40).) When the operator (61) is
applied to ψ at a point 0 next to the upper or lower boundary, ψ_1 or ψ_3
is set equal to zero as required by the boundary conditions. For a point
0 on the line $\eta = \eta_{II}$, ψ_4 is replaced by Ψ_4/g_4 to conform with the
variables used in the region $\eta < \eta_{II}$ (see above).
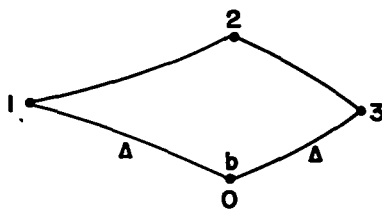
Regular supersonic points.- The arrangement
of points in this case is shown in sketch (f).
Here the adjacent points 1, 2, 3 are chosen to
lie in the region of dependence of the point 0,
which for the present flow is the curvilinear
quadrant opening toward the corner characteristic
and the sonic line.[6] Through application of
the series-expansion procedure in the r,l

Sketch (f)

[6]Note that the increment in r or l from one mesh line to the next
is the same as Δ, the mesh interval on the sonic line (cf. eqs. (15)).

coordinates, the following difference operator is found by approximation to the differential operator (54b):

$$L_\Delta(F) = \frac{[6(r_0 - l_0)]^{2/3}}{\Delta^2} \left[-(F_2 - F_1 - F_3 + F_0) + \frac{\Delta}{6(r_0 - l_0)} (F_3 - F_1) \right] + b_0 F_0$$

(62)

Supersonic points next to corner characteristic.- The situation at a point of this kind is shown in sketch (g). It is known from Guderley's solution for flow over a convex corner (ref. 16) that ψ will have a singularity in the second derivatives at the corner. This means that the series-expansion procedure is not permissible in this case and some other approach must be devised.
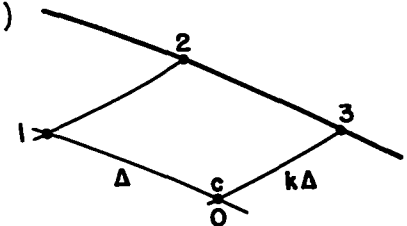
For values of Δ small enough to obtain acceptable results in the numerical solution, equation (59) will ordinarily have reduced to equation (60) by the time the boundary is reached. We need concern ourselves, therefore, only with an expression for L_Δ as applied to ψ. According to Guderley's singular solution, in the vicinity of the corner characteristic the variation of ψ along a line of constant l (such as 03 or 12) is of the form

Sketch (g)

$$\psi \sim (r_{DE} - r)^{4/3}$$

(63)

where r_{DE} is the value of r at the corner. Although Guderley's solution is for the Tricomi equation, the same result may be expected for the exact equation (7). An interpolating function that satisfies condition (63) and may therefore be used as an approximation to ψ in the vicinity of the point 0 is

$$\psi = \left(\frac{r_3 - r}{k\Delta}\right)^{4/3} \left[\psi_0 + \frac{\psi_1 - \psi_0}{\Delta} (l - l_0) \right]$$

Differentiation of this relation and substitution into expression (54b) gives for the difference operator at the point 0

$$L_\Delta(\psi) = \frac{[6(r_0 - l_0)]^{2/3}}{\Delta^2} \left\{ \frac{4}{3k} (\psi_1 - \psi_0) + \frac{\Delta}{6(r_0 - l_0)} \left[\left(1 - \frac{4}{3k}\right) \psi_0 - \psi_1 \right] \right\} + b_0 \psi_0$$

(64)
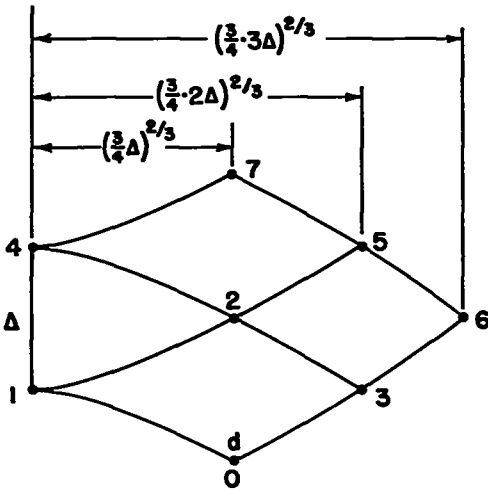
Sketch (h)

Supersonic points next to sonic line.-
A complication arises in this case (see
sketch (h)) from the fact that the deriva-
tives of ψ in the r,l coordinates are
singular on the sonic line (cf. eq. (17)).
As a consequence, a series expansion in
the r,l coordinates, like that employed
at regular supersonic points, cannot be
used here. This difficulty can be over-
come by using an expansion in η,θ coor-
dinates, where the derivatives are regular,
and approximating the differential operator
in the form (54a).

To carry out the approximation, the
truncated Taylor's series for the func-
tion F in the vicinity of the point 0
is taken in the form

$$F = F_0 + (\eta - \eta_0)F_{\eta_0} + (\theta - \theta_0)F_{\theta_0} + \frac{(\eta - \eta_0)^2}{2} F_{\eta\eta_0} +$$

$$(\eta - \eta_0)(\theta - \theta_0)F_{\eta\theta_0} + \frac{(\theta - \theta_0)^2}{2} F_{\theta\theta_0} + \frac{(\eta - \eta_0)^3}{6} F_{\eta\eta\eta_0} \qquad (65)$$

In this connection we note that, for mesh points in the vicinity of 0,
$(\eta - \eta_0)$ is of order $\Delta^{2/3}$ while $(\theta - \theta_0)$ is of order Δ (see eqs. (16)).
This means that the cubic term in $(\eta - \eta_0)$ is of the same order in Δ as
the squared term in $(\theta - \theta_0)$ and must be retained in the series.[7] By
application of the series (65) successively at the points 1 through 7, a
set of simultaneous equations is obtained that can be solved for $F_{\eta\eta_0}$ and
$F_{\theta\theta_0}$. Substitution of the resulting expressions into the differential
operator (54a) gives finally for the difference operator at the point 0

$$L_\Delta(F) = \frac{1}{(3\Delta/4)^{4/3}}\left[\lambda(F_1+F_4) + \sigma(F_3+F_5) + 2\tau F_6 - \left(\frac{\lambda+\sigma}{4} + \frac{9}{16}\right)(F_0+F_7) - \right.$$

$$\left. \frac{3}{2}\left(\lambda + \sigma + \frac{4}{3}\tau - \frac{3}{4}\right)F_2\right] + b_0F_0 \qquad (66)$$

[7]This arises from the fact that, although the expansion is being
carried out in the η,θ variables, the mesh points are still arranged on
lines of constant r and l.

where

$$\lambda = \frac{2^{2/3}(2 - 2^{2/3}) - 3^{2/3}(2 - 3^{2/3})}{6^{2/3}(3^{2/3} - 2^{2/3})}$$

$$\sigma = -\frac{2 - 3^{2/3}}{2^{2/3}(2^{2/3} - 1)(3^{2/3} - 2^{2/3})}$$

$$\tau = \frac{2 - 2^{2/3}}{3^{2/3}(3^{2/3} - 1)(3^{2/3} - 2^{2/3})}$$

When the point O is close to the corner - as at the point d' in sketch (d) - a further complication arises since the points 5, 6, and 7 of sketch (h) are no longer available. As will be seen later, however, analytical knowledge of the nature of ψ where the sonic line approaches the corner characteristic can be used to obtain expressions for ψ_η and ψ_θ at point 2. (Here only ψ is of interest, since at point d' equation (59) will have reduced again to equation (60).) By differentiation of the series (65) with respect to η and θ and application of the resulting expressions at 2, simultaneous equations can again be obtained that can be solved for $\psi_{\eta\eta_0}$ and $\psi_{\theta\theta_0}$. In this way the following formula is obtained for the necessary difference operator when point O is located at d':

$$L_\Delta(\psi) = \frac{1}{(3\Delta/4)^{4/3}}\left[\lambda(\psi_1 - \psi_2) + \sigma(\psi_3 - \psi_2) + \tau(\psi_4 - \psi_2) - \right.$$

$$\frac{1}{4}\left(\lambda + \sigma + \tau + \frac{9}{2}\right)(\psi_0 - \psi_2) + 2\tau\left(\frac{3\Delta}{4}\right)^{2/3}\psi_{\eta_2} +$$

$$\left.\frac{1}{4}\left(\lambda + \sigma - 3\tau - \frac{9}{2}\right)\Delta\psi_{\theta_2}\right] + b_0\psi_0 \qquad (67)$$

where now

$$\lambda = \frac{2^{2/3} + 2^{1/3} - 2}{2^{2/3} - 1}$$

$$\sigma = \frac{2^{1/3}}{\left(2^{2/3} - 1\right)^2}$$

$$\tau = \frac{2^{2/3} - 2}{2^{2/3} - 1}$$
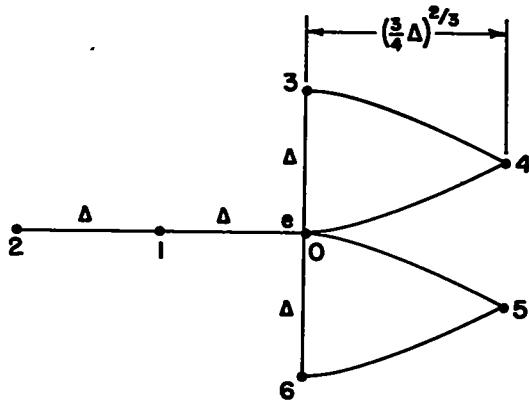
Sketch (i)

Points on sonic line.- The arrangement at a point of this type is shown in sketch (i). The Taylor's series for F as an expansion about point 0 is again taken in the form of equation (65), where now $\eta_0 = 0$. By applying this series at points 1 through 6 and solving the resulting equations for $F_{\eta\eta_0}$, one can write the difference operator, by approximation to equation (54a), as

$$L_\Delta(F) = \frac{1}{\Delta^2 t(t+1)(t+2)} \left[t(t^2 - 1)F_2 - 2t(t^2 - 4)F_1 - \frac{3}{4}(F_3 + F_6) + \right.$$

$$\left. 3(F_4 + F_5) - \left(\frac{9}{2} + 7t - t^3\right)F_0 \right] + b_0 F_0 \tag{68}$$

where t is related to Δ by

$$t = \left(\frac{3}{4}\right)^{2/3} \Delta^{-1/3} \tag{69}$$

Points near intersection of sonic line and corner characteristic.- At the two points near the intersection of the sonic line and corner characteristic (points f_1 and f_2 in sketches (d) and (j)) the difference

operators (68) and (66) cannot be used since the necessary adjacent points are not present. These two points can be eliminated from the problem, however, by use of an interpolating function in the region in question. An appropriate function is provided here by Guderley's singular solution for flow over a convex corner (ref. 16). Though determined for the Tricomi equation, this solution should provide a good approximation to the corresponding solution for the exact equation for small values of η. The details are as follows:

According to Guderley's solution, the variation of ψ in the vicinity of point D of sketch (j) can be represented by

$$\psi = B|\eta|^2 f_{II}(\zeta;2) \qquad (70)$$

where B is a constant and ζ is now defined by

$$\zeta \equiv \frac{9(\theta_D - \theta)^2}{4\eta^3} \qquad (71)$$

The function f_{II}, given originally by Guderley in terms of hypergeometric series, can be represented in closed form by

$$f_{II}(\zeta;2) = |s^2 - 1|^{-2/3}\left[\left(\frac{1}{3} + s\right)(1 - s)^{1/3} - \left(\frac{1}{3} - s\right)(1 + s)^{1/3}\right] \qquad (72)$$

where now

$$s \equiv \frac{\theta_D - \theta}{\sqrt{(\theta_D - \theta)^2 - \frac{4}{9}\eta^3}} = \sqrt{\frac{\zeta}{\zeta - 1}} \qquad (73)$$

To determine the constant B, the function (70) is made to pass through the value of ψ at the mesh point 1 of sketch (j). We thus obtain finally for the interpolating function in the region in question

$$\psi = \frac{\psi_1}{3^{1/3}(\theta_D - \theta)^{4/3}}|\eta|^2 f_{II}(\zeta;2) \qquad (74)$$

Sketch (j)
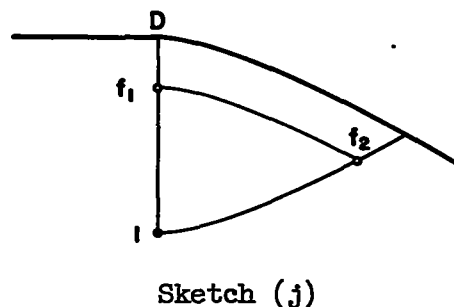
This function is used to eliminate the values of ψ for points f_1 and f_2 wherever these values appear in the finite-difference equations for neighboring points. After differentiation, equation (74) also provides the necessary expressions for the derivatives ψ_{η_2} and ψ_{θ_2} required in equation (67).
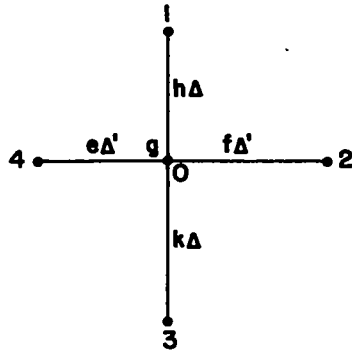
Regular subsonic points in w, θ coordinates.- A typical point, g, of this category is shown in sketch (k). Here provision must be made for an irregular mesh interval in any direction from O as indicated in the sketch by the constants e, f, h, and k. As previously explained, the difference equation is obtained in this case by approximation to equation (1) rather than to equation (59). The result, as obtained by the series-expansion procedure, can be written

Sketch (k)

$$\frac{1+eP}{f(e+f)} \, \Psi_2 + \frac{1-fP}{e(e+f)} \, \Psi_4 + \frac{Q}{hk(h+k)} \, (k\Psi_1 + h\Psi_3) - \left[\frac{e+f+(e^2-f^2)P}{ef(e+f)} + \frac{Q}{hk}\right]\Psi_0 = 0$$

$$(75)$$

where

$$P = \frac{\Delta'}{2w_0} \frac{1 - \dfrac{\gamma-3}{\gamma+1} w_0^2}{1 - \dfrac{\gamma-1}{\gamma+1} w_0^2}$$

$$Q = \left(\frac{\Delta'}{\Delta}\right)^2 \frac{1}{w_0^2} \frac{1 - w_0^2}{1 - \dfrac{\gamma-1}{\gamma+1} w_0^2}$$

For application at points on the line $\eta = \eta_I$ (see sketch (d)), Ψ_2 in equation (75) is replaced by $g_2\Psi_2$ as required by the variables used in the region $\eta > \eta_I$.

Points next to stagnation point.- The use of equation (75) at points next to the stagnation point - as, for example, at point h in sketch (d) - is not practical. This is due to the fact that the final values of Ψ are obtained by taking the difference between two quantities which, according

to the boundary conditions at the stagnation point, are
very nearly equal in this vicinity (see eqs. (3)
through (5)). This difficulty can be overcome as follows:

The situation in the region adjacent to the stag-
nation point is shown in sketch (l). For small values of
w, a solution of equation (1) that satisfies the boundary
condition that $\Psi = 0$ on the surface of the plate (where
Ψ again represents either Ψ^a or Ψ^s) is given by the
series

$$\Psi(w,\theta) = D_1 w\ \sin(\theta + \alpha) + D_2 w^2 \sin[2(\theta + \alpha)] +$$

$$D_3 w^3\left\{\sin[3(\theta + \alpha)] - \frac{D_1}{D_3}\frac{\sin(\theta + \alpha)}{2(\gamma + 1)}\right\} + O(w^4) \qquad (76)$$
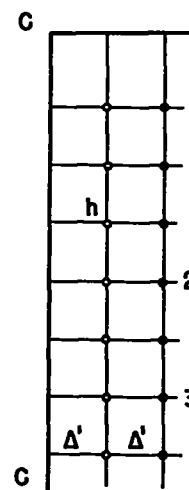
Sketch (l)

Here α is the angle of attack and D_1, D_2, and D_3 are constants. By
writing equation (76) for any three points 1, 2, 3 on the vertical line
$w = 2\Delta'$ and neglecting terms of $O(w^4)$, we obtain three simultaneous
equations for D_1, D_2, and D_3. These equations can be solved to obtain

$$D_1 = D_1(\Psi_1,\Psi_2,\Psi_3) \qquad (77)$$

and similarly for D_2 and D_3. With these relations and equation (76) we
can then express Ψ at any point h on the line $w = \Delta'$ in the form

$$\Psi_h = \Psi_h(\Psi_1,\Psi_2,\Psi_3) \qquad (78)$$

These expressions are used to replace Ψ_4 in the difference equation (75)
when that equation is written for mesh points on the line $w = 2\Delta'$. In
this manner points next to the stagnation point are eliminated from
explicit consideration in the finite-difference scheme. For best accuracy
the points 1, 2, 3 should be placed at approximately equal intervals
between the upper and lower boundaries. If this is done, no difficulty
is found in obtaining satisfactory results without a reduction in mesh
size in the vicinity of the stagnation point.

Distribution of mesh points.- The mesh used for an actual calculation
is not uniform as in sketch (d) but has a different spacing in different
parts of the field. The distribution of mesh interval for the present
solution ($\alpha = 13°$) is shown in figure 6. This particular distribution
involves a total of 880 finite-difference equations. The same distribution

was used for both ψ^a and ψ^s. As in references 3 and 4, the transition
between the various parts of the graded mesh was accomplished by the use
of overlapping fields in essentially the manner described in reference 18.

Solution of Finite-Difference Equations

The solution of the finite-difference equations was obtained by an
iterative process involving both relaxation techniques and step-by-step
procedures. In the first stage of each iteration, the values of ψ for
the column of mesh points immediately to the right of the sonic line (as
obtained from an initial guess or from the previous iteration) are con-
sidered fixed. On the basis of these values, a boundary-value problem
is then solved for the points in the subsonic field and on the sonic line.
This is done by the use of standard relaxation techniques (see, e.g.,
refs. 19, 20, and 21). In the second stage of the iteration the values
of ψ obtained on the sonic line as a result of the first stage are used
as the initial values for an initial-value problem in the supersonic field.
This problem is solved in simple step-by-step fashion proceeding along
the characteristics running from the sonic line to the limiting character-
istic. This is done first for the characteristic adjacent to the corner
and then for succeeding characteristics in the interior of the flow. By
means of this procedure one obtains a new set of values for ψ at the
points immediately to the right of the sonic line. Those values are now
considered fixed again, and the entire process is repeated. This con-
tinues until a consistent solution is obtained for the complete set of
finite-difference equations.

The numerical work for the present solution was performed entirely
on a desk calculator. In the initial stages of the iteration process the
relaxation solution of the subsonic field was rarely carried to completion
at any given stage. Over- and under-relaxation were, in fact, found use-
ful to counteract the changes fed back by the subsequent work in the super-
sonic region. Within the subsonic field, block relaxation was used exten-
sively. Such devices were, in fact, essential to the solution of the
problem in a practicable length of time.

The results of the calculations are shown in figures 7 to 9 as contour
maps of Ψ in w,θ coordinates. Numerical values are also given in
table II at the end of the report. For the reasons explained in part I,
the calculations were made for a value of γ of 1.405. The results for
Ψ^a in figure 7 and table II correspond to $A^a = 100$; the results for Ψ^s
in figure 8 and table II to $A^s = 1,000$. These values, which fix the
strength of the singularities, were chosen to give a convenient level for
the dependent variable throughout most of the field and to provide an
absolute value of approximately 1 for the constant C in equation (4).
For both solutions the work was done to integer values of ψ in most of
the field, and the residuals in the relaxation work were eliminated to
within ± 2 (with due care that residuals in any given area were not pre-
dominately of the same sign). Near the boundaries, where ψ is small,

the work was done with values of ψ to two decimal places, and the residuals were eliminated to within ±0.02. The final solution for Ψ, given in figure 9 and table II, was calculated from equation (4) with C = -1.007. This figure was arrived at from the relation

$$C = -\frac{D_1{}^a}{D_1{}^s}$$

which is obtained by substituting equation (76) into equation (5). The values of $D_1{}^a$ and $D_1{}^s$ were computed from an equation of the form (77), as obtained in the treatment of the mesh points next to the stagnation point.

Transformation to Physical Plane

The transformation from the hodograph plane to the physical plane is accomplished by integration of equations (51) or (52). Since the necessary integrations are chiefly along lines of constant w, θ, r, or l, the equations simplify considerably in application. The actual integration was carried out in the present work by mechanical means on the basis of plots of the appropriate integrand. The values of the derivatives of Ψ that appear in the various integrands were found by numerical differentiation of the values listed in table II. A detailed explanation of the procedure as applied to a similar problem has been given in reference 3, and little more need be said here. It should be noted, however, that when the integration of equations (52) is performed along a line of constant r or l, the expression to be integrated reduces to the form $f(w,\theta)d\Psi$. In this case, therefore, no numerical differentiation of Ψ is required, which is advantageous with regard to the accuracy of the final result.

With the distribution of w known on the lower surface of the plate, the corresponding pressures can be calculated from the usual isentropic relations. This follows from the fact that the flow on the lower surface is irrotational (see Description of Flow Field).

CHARACTERISTICS CONSTRUCTION OF FLOW OVER REGION OF SEPARATION

As explained in part I, the calculation of the region of separation on the upper surface was accomplished on an electronic computer by means of a numerical method of characteristics. The method employed was based on the original Prandtl-Busemann procedure for two-dimensional irrotational flow (see, e.g., ref. 8). For the results shown in figure 1 the increment in stream angle between successive points in the characteristics net was taken as 1° throughout most of the field. In a small region adjacent to

the leading edge this increment was reduced to 0.2°. A check calculation
using an increment of 2° outside the latter region gave results negligibly
different from those obtained with 1°. With the 1° increment, the number
of calculated points in the region of dependence of the separated stream-
line was approximately 6600. To obtain the required initial data on the
limiting wave (i.e., x/c and y/c as functions of r) it was necessary to
interpolate between the values obtained from the mesh points used in the
transonic calculation (see fig. 6). This was done graphically over most
of the range. Near the leading edge, however, the interpolation was done
analytically on the basis of an interpolating function compatible with
the nature of the singularity in the vicinity of the corner characteristic.
The values of the initial data are listed in table III for anyone who may
wish to calculate the flow over an airfoil with another type of upper
surface.

Ames Aeronautical Laboratory
        National Advisory Committee for Aeronautics
                Moffett Field, Calif., May 7, 1956

APPENDIX

NOTATION

Primary Symbols

a_*	critical speed (i.e., speed at which speed of flow and speed of sound are equal)
A	constant determining strength of singularity
b	function of η in differential equation for ψ (see eqs. (7) and (12))
b_0, b_1, b_2	constants in series expansion for b (see eq. (13))
c	chord of plate
C	constant in superposition equation (see eqs. (4) and (5))
C_p	pressure coefficient, $\dfrac{p - p_\infty}{q_\infty}$
D_1, D_2, D_3	constants in series solution for Ψ in vicinity of stagnation point (see eqs. (76) and (77))
e, f, h, k	length of irregular mesh intervals relative to that of basic interval
$f_I(\zeta;n),$ $f_{II}(\zeta;n)$	functions appearing in singular solutions of Tricomi equation (see eqs. (19) and (70))
F	general symbol for variable in linear operator (may represent ψ, M, or X)
g	function of w in transformation from Ψ to ψ (see eqs. (6) and (11))
g_i, h_i	undefined functions of ζ
i	index of summation (see eq. (22))
I	integral defined by equation (49)
$L_\partial(\ )$	differential operator (see eq. (54))
$L_\Delta(\ )$	difference operator approximating $L_\partial(\ )$

m   maximum value of index i

M   quantity introduced in equation (56) as shorthand notation
                        for quantities appearing in equations (36) and (39)

n   exponent of $|\eta|$ in singular solutions of Tricomi equation
                        (see eqs. (19) and (70))

p   static pressure

p_t total pressure

p_i, q_i constants in solution of equation for $\hat{\psi}_i$ (see eq. (30))

q   dynamic pressure

r, l characteristic coordinates (see eqs. (15) and (16))

s   any length in flow field; also function of η and θ defined
                        by equation (42)

$\left.\begin{array}{l}(\text{sign } \eta), \\ (\text{sign } \theta)\end{array}\right\}$ quantities with absolute value 1 and sign of η or θ

t   index of summation (see eq. (26))

T( )   Tricomi operator (see eq. (18))

w   speed of flow made dimensionless through division by critical
                        speed

x,y   Cartesian coordinates (x in direction of free stream, y
                        vertical, origin at leading edge of plate)

x'   distance along plate measured aft from leading edge

α angle of attack

β function of w (see eq. (53))

γ ratio of specific heats (1.405 in numerical work)

$\left[\delta\left(\dfrac{y}{c}\right)\right]_\infty$ dimensionless distance in free stream between given stream-
                        line and stagnation streamline

Δ basic mesh interval in η and θ

Δ' basic mesh interval in w

ζ	function of η and θ defined by equation (20)
η	function of w in transformation from Ψ to ψ (see eq. (10))
θ	inclination of flow measured counterclockwise from free-stream direction
ρ	density of fluid
ρ_t	total density of fluid
χ	function appearing in solution for ψ (see eq. (22))
ψ	transformed stream function (see eq. (6))
$\tilde{\psi}$	solution representing free-stream singularity for Tricomi equation (see eq. (19))
$\hat{\psi}_1$	singular correction functions (see eq. (22))
$\bar{\psi}$	function appearing in solution for $\hat{\psi}_1$ (see eqs. (27), (28), and (30))
Ψ	stream function

Subscripts

∞	conditions in free stream
s	conditions on separated streamline
max	values corresponding to maximum speed (i.e., to speed attained by expansion to a vacuum)
I,II	values of η and w at change from η to w coordinate in finite-difference mesh
0,1,2,etc.	value at prescribed mesh point

Superscripts

a	quantities pertaining to solution with antisymmetric singularity
s	quantities pertaining to solution with symmetric singularity
( )',( )"	first and second derivatives of function with respect to its argument

REFERENCES

1. Guderley, Gottfried: The Flow Over a Flat Plate With a Small Angle
      of Attack at Mach Number 1.   Jour. Aero. Sci., vol. 21, no. 4,
      Apr. 1954, pp. 261-274.

2. Frankl, F.:   Investigation of the Theory of Wings of Infinite Span
      Moving at the Speed of Sound. Doklady Akad. Nauk SSSR, vol. 57,
      no. 7, 1947, pp. 661-664.

3. Vincenti, Walter G., and Wagoner, Cleo B.:   Transonic Flow Past a
      Wedge Profile With Detached Bow Wave. NACA Rep. 1095, 1952.
      (Supersedes NACA TN's 2339 and 2588)

4. Vincenti, Walter G., and Wagoner, Cleo B.:   Theoretical Study of the
      Transonic Lift of a Double-Wedge Profile With Detached Bow Wave.
      NACA Rep. 1180, 1954.   (Supersedes NACA TN 2832)

5. Liepmann, H. W., and Bryson, A. E., Jr.:   Transonic Flow Past Wedge
      Sections. Jour. Aero. Sci., vol. 17, no. 12, Dec. 1950, pp. 745-755.
      (Also published as C.I.T., Guggenheim Aero. Lab. Pub. 267)

6. Guderley, Gottfried: Two-Dimensional Flow Patterns with a Free-
      Stream Mach Number Close to One. USAF, WADC, AF Tech. Rep. No. 6343,
      May 1951.

7. Guderley, G., and Yoshihara, H.:   The Flow over a Wedge Profile at
      Mach Number 1. Jour. Aero. Sci., vol. 17, no. 11, Nov. 1950,
      pp. 723-735.

8. Guderley, G.:   Monograph on the Theory of Characteristics. Transla-
      tion No. RAT-4, Douglas Aircraft Co., Inc., Santa Monica, Calif.,
      Sept. 1, 1947.

9. Durand, W. F.:   Fluid Mechanics, Part I.   Div. B of Aerodynamic
      Theory, vol. I, W. F. Durand, ed., Julius Springer (Berlin), 1934,
      pp. 159, 184-185.

10. Courant, R., and Friedrichs, K. O.:   Supersonic Flow and Shock Waves.
      Interscience Pub., Inc., 1948.

11. Bickley, W. G.:   Some Exact Solutions of the Equations of Steady
      Homentropic Flow of an Inviscid Gas. Chap. V of Modern Developments
      in Fluid Dynamics; High Speed Flow, vol. I, L. Howarth, ed.,
      Oxford Univ. Press, 1953.

12. Guderley, Gottfried: Transonic Simplifications of the Hodograph
      Equation. WADC Tech. Rep. 53-183, Wright-Patterson Air Force
      Base, June 1953.

13. Wood, George P.: Experiments on Transonic Flow Around Wedges. NACA TN 2829, Nov. 1952.

14. Sauer, Robert: Introduction to Theoretical Gas Dynamics. Trans. by Freeman K. Hill and Ralph A. Alpher. J. W. Edwards, Ann Arbor, 1947.

15. Guderley, Gottfried, and Yoshihara, Hideo: Two-Dimensional Unsymmetric Flow Patterns at Mach Number 1. Jour. Aero. Sci., vol. 20, no. 11, Nov. 1953, pp. 757-768.

16. Guderley, K. Gottfried: Singularities at the Sonic Velocity. Tech. Rep. F-TR-1171-ND, Air Materiel Command, Wright-Patterson Air Force Base, Tech. Intelligence, June 1948.

17. Woods, L. C.: The Relaxation Treatment of Singular Points in Poisson's Equation. Quar. Jour. Mech. and Appl. Math., vol. VI, pt. 2, June 1953, pp. 163-185.

18. Tasny-Tschiassny, L.: The Triangulation of a Two-Dimensional Continuum for the Purpose of the Approximate Solution of Second-Order Partial Differential Equations. Jour. App. Phys., vol. 20, no. 5, May 1949, pp. 419-424.

19. Fox, L.: A Short Account of Relaxation Methods. Quart. Jour. Mech. and Appl. Math., vol. I, pt. 3, Sept. 1948, pp. 253-280.

20. Shaw, F. S.: An Introduction to Relaxation Methods. Dover Pub., Inc., 1953.

21. Allen, D. N. de G.: Relaxation Methods. McGraw-Hill Book Co., Inc., 1954.

TABLE I.- VALUES OF w , η , g , AND b $(\gamma = 1.405)$

w	η	g	-b
0	-∞	∞	0
.109	-2.037	1.736	---
.164	-1.745	1.671	---
.218	-1.524	1.615	---
.272	-1.343	1.566	---
.326	-1.190	1.520	---
.379	-1.056	1.477	---
.432	-.935	1.436	.261
.484	-.826	1.395	.300
.539	-.725	1.356	.343
.585	-.631	1.317	.388
.635	-.545	1.280	.442
.684	-.463	1.243	.482
.732	-.386	1.206	.540
.779	-.313	1.170	.593
.825	-.245	1.135	.652
.871	-.179	1.100	.712
.915	-.116	1.065	.777
.958	-.057	1.035	.850
1.000	0	1.000	.918
1.067	.088	.947	1.041
1.107	.140	.917	1.125
1.141	.183	.890	1.200
1.200	.258	.842	1.339
1.252	.323	.800	1.475
1.323	.409	.744	1.685
1.428	.536	.660	2.055
1.522	.650	.585	2.531
1.609	.754	.515	3.045
1.690	.851	.452	3.641
1.765	.943	.394	4.348
1.836	1.031	.340	5.193
1.902	1.115	.291	6.378
1.964	1.197	.246	7.461
2.022	1.275	.204	8.986
2.076	1.351	.170	10.894
2.127	1.425	.138	13.301
2.173	1.497	.109	16.406
2.215	1.568	.084	20.468
2.254	1.637	.065	25.904
2.289	1.704	.048	33.394
2.389	1.950	.011	---
2.437	2.252	0	∞

TABLE II.- Ψ^a, Ψ^s, AND Ψ AS FUNCTIONS OF w AND θ ($A^a = 100$, $A^s = 1000$, $\gamma = 1.405$)

w	θ	Ψ^a	Ψ^s	Ψ
1.000	2.80	1.87	1.82	0.067
	2.70	4.15	4.03	.148
	2.60	6.82	6.60	.247
	2.50	9.80	9.46	.361
	2.40	13.02	12.55	.493
	2.20	20.4	19.6	.82
	2.00	29.4	28.0	1.25
	1.80	40.5	38.5	1.87
	1.60	55.2	52.0	2.83
	1.40	75.5	70.5	4.49
	1.20	105.6	97.5	7.39
	1.00	153.2	138.5	13.7
	.90	191	172	17.8
	.80	241	214	25.5
	.70	314	272	40.0
	.60	424	353	68.5
	.50	597	475	119
	.45	724	557	163
	.40	897	667	225
	.35	1,147	813	328
	.30	1,505	1,014	484
	.25	2,067	1,300	758
	.20	3,037	1,728	1,297
	.15	4,957	2,430	2,510
	.10	9,835	3,784	6,024
	.05	31,496	7,440	24,002
	0			
	-.05	-29,620	6,770	-36,439
	-.10	-7,814	2,841	-10,675
	-.15	-2,748	1,217	-3,974
	-.20	-678	301	-981
.963	.45	824	628	191
	.40	1,024	755	264
	.35	1,317	924	386
	.30	1,751	1,158	584
	.25	2,428	1,493	925
	.20	3,599	2,004	1,581
	.15	6,012	2,854	3,137
	.10	12,349	4,548	7,768
	.05	42,538	9,348	33,123
	0	966	57,782	-57,233
	-.05	-40,548	8,738	-49,348
	-.10	-10,256	3,601	-13,832
	-.15	-3,644	1,590	-5,245
	-.20	-953	453	-1,409
.927	2.80	2.73	2.65	.098
	2.70	5.59	5.43	.201
	2.60	8.82	8.55	.322
	2.50	12.38	11.96	.461
	.90	237	212	23.0
	.80	300	264	34.0
	.70	393	336	54.6
	.60	534	440	90.9
	.50	758	598	156
	.45	927	703	219
	.40	1,157	845	305
	.35	1,490	1,037	445
	.30	1,984	1,306	669
	.25	2,764	1,690	1,061
	.20	4,131	2,279	1,836
	.15	6,942	3,271	3,648
	.10	14,226	5,232	8,956
	.05	44,279	10,532	33,671
	0	1,023	27,701	-26,878
	-.05	-42,174	9,972	-52,219
	-.10	-11,957	4,279	-16,267
	-.15	-4,412	1,951	-6,377
	-.20	-1,204	595	-1,803

w	θ	Ψ^a	Ψ^s	Ψ
0.892	0.45	1,029	779	245
	.40	1,286	937	343
	.35	1,657	1,152	497
	.30	2,207	1,450	746
	.25	3,073	1,882	1,179
	.20	4,574	2,532	2,024
	.15	7,554	3,617	3,911
	.10	14,590	5,685	8,864
	.05	34,178	10,423	23,679
	0	1,078	17,625	-16,674
	-.05	-31,963	9,895	-41,930
	-.10	-12,202	4,722	-16,957
	-.15	-4,865	2,238	-7,120
	-.20	-1,387	704	-2,094
.856	2.80	3.63	3.53	.131
	2.70	7.17	6.95	.259
	2.60	11.03	10.68	.405
	2.50	15.24	14.72	.569
	2.40	19.78	19.05	.760
	2.20	30.1	29.0	1.22
	2.00	42.9	40.9	1.86
	1.80	58.9	55.9	2.79
	1.60	80.5	75.7	4.23
	1.40	110.7	103.1	6.81
	1.20	156.4	143.5	11.8
	1.00	230.2	207.2	21.4
	.90	286	257	27
	.80	363	319	42
	.70	477	406	68
	.60	648	531	113
	.50	921	721	195
	.45	1,127	851	270
	.40	1,407	1,026	373
	.35	1,806	1,259	538
	.30	2,393	1,583	799
	.25	3,299	2,046	1,238
	.20	4,937	2,735	2,182
	.15	7,637	3,841	3,768
	.10	13,230	5,799	7,389
	.05	21,741	9,357	12,317
	0	1,126	12,538	-11,502
	-.05	-19,429	8,845	-28,338
	-.10	-10,737	4,823	-15,594
	-.15	-4,816	2,404	-7,238
	-.20	-1,441	776	-2,222
.821	.45	1,213	921	285
	.40	1,510	1,107	395
	.35	1,923	1,355	557
	.30	2,521	1,694	814
	.25	3,418	2,171	1,231
	.20	4,847	2,862	1,965
	.15	7,195	3,914	3,253
	.10	10,830	5,572	5,219
	.05	13,050	7,985	5,007
	0	1,164	9,444	-8,348
	-.05	-10,663	7,483	-18,198
	-.10	-8,260	4,584	-12,878
	-.15	-4,288	2,427	-6,732
	-.20	-1,360	800	-2,166
.788	2.80	4.57	4.43	.165
	2.70	8.82	8.54	.320
	2.60	13.37	12.94	.492
	2.50	18.28	17.64	.684
	.90	336	301	33
	.80	425	374	49
	.70	557	474	79
	.60	753	618	130

w	θ	Ψ^a	Ψ^s	Ψ
0.788	0.50	1,060	834	220
	.45	1,285	983	295
	.40	1,587	1,178	401
	.35	2,000	1,434	555
	.30	2,578	1,777	789
	.25	3,412	2,247	1,148
	.20	4,635	2,904	1,710
	.15	6,376	3,838	2,510
	.10	8,326	5,140	3,149
	.05	8,033	6,685	1,300
	0	1,189	7,359	-6,223
	-.05	-5,597	6,186	-11,828
	-.10	-5,715	4,145	-9,890
	-.15	-3,440	2,318	-5,774
	-.20	-1,159	781	-1,945
.755	.45	1,338	1,036	294
	.40	1,636	1,236	392
	.35	2,031	1,491	529
	.30	2,563	1,826	724
	.25	3,290	2,272	1,002
	.20	4,254	2,865	1,369
	.15	5,404	3,648	1,731
	.10	6,209	4,616	1,560
	.05	5,250	5,573	-363
	0	1,199	5,869	-4,712
	-.05	-2,801	5,080	-7,918
	-.10	-3,601	3,620	-7,248
	-.15	-2,506	2,118	-4,639
	-.20	-896	726	-1,627
.724	2.80	5.52	5.34	.199
	2.70	10.54	10.18	.381
	2.60	15.84	15.31	.580
	2.50	21.51	20.72	.804
	2.40	27.60	26.55	1.057
	2.20	41.4	39.8	1.67
	2.00	58.4	55.7	2.52
	1.80	80.0	75.8	3.77
	1.60	109.0	102.6	5.7
	1.40	149.9	139.7	9.2
	1.20	211.3	194.2	15.7
	1.00	309.9	279.7	28.1
	.90	383	343	38
	.80	482	424	55
	.70	625	535	86
	.60	833	694	134
	.50	1,149	921	222
	.45	1,368	1,077	284
	.40	1,651	1,275	366
	.35	2,014	1,522	481
	.30	2,483	1,838	631
	.25	3,076	2,244	816
	.20	3,778	2,756	1,003
	.15	4,458	3,381	1,052
	.10	4,680	4,073	579
	.05	3,669	4,650	-1,015
	0	1,190	4,745	-3,588
	-.05	-1,246	4,165	-5,441
	-.10	-2,123	3,088	-5,233
	-.15	-1,663	1,866	-3,542
	-.20	-630	649	-1,284
.693	.45	1,378	1,106	265
	.40	1,638	1,296	332
	.35	1,958	1,530	417
	.30	2,350	1,820	517
	.25	2,810	2,177	617
	.20	3,289	2,603	668
	.15	3,644	3,084	538

Note: All values of θ in radians.

TABLE II.- Ψ^a, Ψ^s, AND Ψ AS FUNCTIONS OF w AND θ ($A^a = 100$, $A^s = 1000$, γ = 1.405) - Continued

w	θ	Ψ^a	Ψ^s	Ψ
0.693	0.10	3,580	3,561	-8
	.05	2,740	3,899	-1,187
	0	1,165	3,883	-2,746
	-.05	-375	3,423	-3,822
	-.10	-1,110	2,599	-3,727
	-.15	-997	1,606	-2,614
	-.20	-400	564	-967
.662	2.80	6.49	6.26	.232
	2.70	12.31	11.88	.444
	2.60	18.41	17.75	.672
	2.50	24.87	23.94	.924
	.90	423	381	40
	.80	528	467	57
	.70	674	585	85
	.60	878	745	129
	.50	1,172	970	194
	.45	1,363	1,119	237
	.40	1,593	1,297	287
	.35	1,865	1,512	341
	.30	2,177	1,768	397
	.25	2,515	2,071	428
	.20	2,819	2,412	389
	.15	2,974	2,768	185
	.10	2,801	3,087	-309
	.05	2,152	3,270	-1,142
	0	1,121	3,193	-2,094
	-.05	116	2,810	-2,714
	-.10	-460	2,160	-2,635
	-.15	-517	1,353	-1,880
	-.20	-221	478	-702
.632	.45	1,328	1,116	204
	.40	1,585	1,280	236
	.35	1,749	1,473	266
	.30	1,989	1,694	282
	.25	2,223	1,942	267
	.20	2,403	2,207	181
	.15	2,445	2,462	-34
	.10	2,248	2,665	-436
	.05	1,760	2,748	-1,007
	0	1,062	2,639	-1,596
	-.05	381	2,311	-1,946
	-.10	-63	1,785	-1,860
	-.15	-198	1,125	-1,330
	-.20	-96	399	-498
.604	2.80	7.42	7.15	.263
	2.70	14.04	13.53	.501
	2.60	20.90	20.14	.756
	2.50	28.15	27.11	1.036
	2.40	35.90	34.50	1.349
	2.20	53.4	51.2	2.11
	2.00	74.7	71.2	3.14
	1.80	101.7	96.5	4.64
	1.60	137.5	129.7	6.9
	1.40	187.4	175.2	10.9
	1.20	260.1	240.6	17.8
	1.00	372.2	339.7	30.1
	.90	450	409	38
	.80	555	497	54
	.70	694	613	76
	.60	879	766	108
	.50	1,126	970	150
	.45	1,273	1,098	168
	.40	1,437	1,245	184
	.35	1,614	1,411	193

w	θ	Ψ^a	Ψ^s	Ψ
0.604	0.30	1,792	1,596	184
	.25	1,948	1,794	141
	.20	2,044	1,992	38
	.15	2,027	2,169	-158
	.10	1,844	2,289	-462
	.05	1,478	2,308	-848
	0	990	2,185	-1,211
	-.05	510	1,900	-1,404
	-.10	164	1,466	-1,312
	-.15	1	924	-930
	-.20	-16	328	-346
.576	.45	1,210	1,071	131
	.40	1,344	1,199	135
	.35	1,481	1,342	130
	.30	1,609	1,492	106
	.25	1,708	1,646	51
	.20	1,750	1,790	-53
	.15	1,704	1,908	-217
	.10	1,544	1,969	-440
	.05	1,264	1,946	-697
	0	913	1,819	-919
	-.05	564	1,571	-1,019
	-.10	285	1,208	-933
	-.15	117	757	-644
	-.20	32	265	-236
.550	2.80	8.34	8.03	.292
	2.70	15.75	15.16	.555
	2.60	23.39	22.53	.835
	2.50	31.39	30.28	1.138
	.90	467	429	35
	.80	565	514	47
	.70	689	621	63
	.60	843	757	81
	.50	1,032	931	94
	.40	1,243	1,141	94
	.30	1,434	1,377	47
	.20	1,504	1,594	-102
	.10	1,307	1,689	-394
	0	831	1,517	-697
	-.10	336	999	-670
.498	2.80	9.21	8.87	.318
	2.60	25.71	24.73	.900
	2.40	43.81	42.08	1.58
	2.20	64.6	62.0	2.43
	2.00	89.6	85.6	3.57
	1.80	120.7	114.9	5.16
	1.60	161.1	152.5	7.5
	1.40	215.3	202.7	11.1
	1.20	290.7	271.9	16.8
	1.00	398.4	370.4	25.4
	.90	469	436	30
	.80	556	513	39
	.70	660	609	47
	.60	780	723	51
	.50	913	856	51
	.40	1,043	1,001	34
	.30	1,134	1,149	-24
	.20	1,127	1,252	-133
	.10	968	1,246	-286
	0	672	1,068	-404
	-.10	343	686	-349
.450	.90	460	433	24
	.80	532	501	28

w	θ	Ψ^a	Ψ^s	Ψ
0.450	0.70	615	581	30
	.60	704	670	29
	.50	793	767	20
	.40	867	862	-2
	.30	901	943	-50
	.20	867	978	-118
	.10	740	928	-195
	0	535	764	-235
	-.10	296	481	-188
.405	2.80	10.72	10.32	.351
	2.60	29.80	28.68	.984
	2.40	50.44	48.51	1.71
	2.20	73.8	70.9	2.58
	2.00	101.2	96.9	3.69
	1.80	134.6	128.6	5.15
	1.60	176.1	167.8	7.1
	1.40	229.2	218.0	9.7
	1.20	297.9	283.0	12.8
	1.00	386.5	367.7	16.2
	.90	439	420	16
	.80	497	477	16
	.70	560	541	15
	.60	623	608	10
	.50	678	674	-1
	.40	714	730	-21
	.30	719	767	-54
	.20	675	763	-93
	.10	573	697	-129
	0	421	557	-140
	-.10	241	344	-107
.362	.90	412	400	9
	.80	458	446	8
	.70	504	495	5
	.60	546	542	1
	.50	576	585	-13
	.40	591	613	-27
	.30	577	622	-49
	.20	534	598	-69
	.10	451	530	-83
	0	333	415	-85
	-.10	194	254	-62
.323	2.80	11.75	11.33	.355
	2.60	32.57	31.40	.990
	2.40	54.81	52.81	1.69
	2.20	79.45	76.48	2.50
	2.00	107.63	103.50	3.47
	1.80	140.70	135.16	4.62
	1.60	180.15	172.95	5.95
	1.40	227.57	218.62	7.38
	1.20	284.13	273.65	8.51
	1.00	349.27	338.43	8.40
	.80	418.06	409.99	5.12
	.60	476.29	477.25	-4.40
	.40	493.70	513.63	-23.63
	.20	430.05	475.01	-48.39
	0	264.98	315.38	-52.67
.200	2.80	11.28	10.94	.262
	2.60	31.09	30.16	.720
	2.40	51.57	50.04	1.18
	2.20	73.12	70.97	1.65
	2.00	96.06	93.30	2.10
	1.80	120.59	117.27	2.48
	1.60	146.59	142.85	2.71

TABLE II.- Ψ^a, Ψ^s, AND Ψ AS FUNCTIONS OF w AND θ (A^a = 100, A^s = 1000, γ = 1.405) - Continued

w	θ	Ψ^a	Ψ^s	Ψ	w	θ	Ψ^a	Ψ^s	Ψ	w	θ	Ψ^a	Ψ^s	Ψ
0.200	1.40	173.48	169.61	2.65	1.218	2.80	.0496	.0483	.00178	1.325	.275	345	266	77
	1.20	199.87	196.35	2.11		2.70	1.024	.997	.0352		.225	428	319	106
	1.00	223.12	220.72	.811		2.60	2.408	2.339	.0843		.175	545	389	153
	.80	238.92	238.72	-1.52		2.50	4.077	3.947	.1454	1.357	2.70	.0391	.0380	.00140
	.60	241.05	244.25	-4.96		2.40	5.961	5.757	.2173		2.60	.788	.767	.0270
	.40	222.09	229.31	-8.87		2.30	8.005	7.724	.2997		2.50	1.851	1.797	.0648
	.20	176.14	186.15	-11.35		2.20	10.26	9.88	.392		2.40	3.127	3.028	.1116
	0	103.42	111.87	-9.255		2.10	12.64	12.16	.502		2.30	4.558	4.403	.1663
1.083	.425	578	447	128		2.00	15.25	14.59	.623		2.20	6.096	5.883	.2286
	.375	715	535	176		1.90	18.18	17.34	.767		2.10	7.78	7.50	.298
	.325	908	650	254		1.80	21.41	20.42	.922		2.00	9.54	9.18	.381
	.275	1,182	807	369		1.70	24.95	23.67	1.139		1.90	11.45	10.95	.470
	.225	1,610	1,024	579		1.60	28.96	27.33	1.38		1.80	13.59	12.93	.574
	.175	2,339	1,352	978		1.50	33.72	31.72	1.71		1.70	15.93	15.16	.698
	.125	3,759	1,878	1,867		1.40	39.32	36.80	2.14		1.60	18.47	17.49	.845
	.075	7,229	2,882	4,326		1.30	45.81	42.80	2.70		1.50	21.35	20.11	1.03
	.025	21,717	5,456	16,221		1.20	53.81	49.92	3.48		1.40	24.75	23.28	1.26
	-.025	-20,119	4,839	-24,993		1.10	63.71	58.82	4.45		1.30	28.76	26.92	1.59
	-.075	-5,513	2,044	-7,572		1.00	76.57	70.02	6.04		1.20	33.44	31.22	2.00
	-.125	-1,915	853	-2,775		.90	92.18	83.34	8.25		1.10	39.22	36.35	2.57
	-.175	-414	184	-598		.80	114.6	103.0	10.8		1.00	46.40	42.79	3.30
1.138	2.85	.0579	.0564	.00208		.70	144.5	128.3	15.2		.90	55.79	50.94	4.48
	2.75	1.215	1.183	.048		.60	188.0	163.2	23.6		.80	67.23	60.66	6.13
	2.65	2.847	2.765	.0997		.50	253.8	211.8	40.5		.70	83.8	75.2	8.0
	2.55	4.809	4.655	.1716		.40	357	285	70		.60	106.1	94.0	11.5
	2.45	7.026	6.784	.2560		.35	433	335	95		.50	138.4	119.9	17.7
	2.35	9.433	9.102	.3533		.30	534	401	131		.40	187.9	156.2	30.6
	2.25	12.10	11.65	.462		.25	679	487	189		.30	266	210	54
	2.15	14.93	14.35	.593		.20	883	604	276		.25	322	248	73
	2.05	18.03	17.24	.736		.15	1,206	766	435		.20	401	298	101
	1.95	21.55	20.55	.907		.10	1,750	1,008	734	1.387	.225	301	231	68
	1.85	25.42	24.25	1.113		-.10	-306	136	-443	1.417	2.65	.0352	.0342	.00126
	1.75	29.67	28.19	1.355	1.257	.325	400	309	88		2.55	.703	.684	.0242
	1.65	34.52	32.59	1.65		.275	495	371	122		2.45	1.648	1.601	.0577
	1.55	40.26	37.91	2.04		.225	629	451	175		2.35	2.778	2.690	.0992
	1.45	47.03	44.02	2.56		.175	820	560	256		2.25	4.037	3.901	.1474
	1.35	54.86	51.24	3.22		.125	1,119	709	406		2.15	5.385	5.198	.2020
	1.25	64.51	59.86	4.14	1.292	2.75	.0436	.0424	.00156		2.05	6.86	6.60	.263
	1.15	76.39	70.56	5.30		2.65	.889	.866	.0305		1.95	8.38	8.06	.335
	1.05	91.84	84.02	7.21		2.55	2.091	2.031	.0731		1.85	10.03	9.57	.411
	.95	110.55	100.02	9.80		2.45	3.538	3.426	.1263		1.75	11.87	11.29	.500
	.85	137.3	123.7	12.7		2.35	5.169	4.993	.1884		1.65	13.87	13.18	.608
	.75	173.1	153.7	18.4		2.25	6.93	6.688	.2597		1.55	16.04	15.19	.736
	.65	224.7	195.3	28.0		2.15	8.87	8.54	.339		1.45	18.48	17.42	.890
	.55	303.0	253.1	48.1		2.05	10.90	10.49	.434		1.35	21.38	20.12	1.10
	.45	425	339	83		1.95	13.12	12.55	.538		1.25	24.83	23.23	1.38
	.40	516	399	114		1.85	15.61	14.87	.659		1.15	28.82	26.89	1.73
	.35	636	478	155		1.75	18.34	17.46	.804		1.05	33.78	31.29	2.23
	.30	809	580	225		1.65	21.32	20.22	.974		.95	39.96	36.83	2.88
	.25	1,050	719	326		1.55	24.70	23.28	1.18		.85	48.08	43.85	3.91
	.20	1,433	911	516		1.45	28.70	26.99	1.46		.75	57.98	52.26	5.35
	.15	2,078	1,198	871		1.35	33.41	31.28	1.83		.65	72.4	65.0	6.9
	.10	3,319	1,667	1,640		1.25	38.87	36.30	2.31		.55	91.8	81.2	10.0
	.05	6,370	2,550	3,801		1.15	45.64	42.32	2.97		.45	120.2	103.9	15.6
	-.05	-4,824	1,794	-6,630		1.05	54.01	49.84	3.80		.35	163.4	135.6	26.8
	-.10	-1,666	742	-2,414		.95	64.91	59.31	5.17		.25	232	183	48
	-.15	-364	161	-526		.85	78.17	70.62	7.04	1.470	2.60	.0319	.0310	.00115
1.179	.375	469	364	103		.75	97.2	87.4	9.2		2.50	.632	.615	.0217
	.325	581	436	142		.65	123.0	109.0	13.1		2.40	1.477	1.435	.0517
	.275	736	529	204		.55	160.0	138.9	20.2		2.30	2.481	2.403	.0887
	.225	958	656	298		.45	216.6	180.5	34.8		2.20	3.596	3.475	.1313
	.175	1,307	830	471		.35	305	243	60		2.10	4.781	4.615	.1795
	.125	1,895	1,094	794		.30	370	286	82		2.00	6.07	5.84	.233
	.075	3,017	1,520	1,486		.25	458	343	113		1.90	7.39	7.10	.295
	-.075	-1,505	675	-2,185		.20	584	418	163		1.80	8.82	8.42	.361
	-.125	-331	147	-478		.15	761	518	239					

TABLE II.- y^a, y^s, AND y AS FUNCTIONS OF w AND θ ($A^a = 100$, $A^s = 1000$, $\gamma = 1.405$) - Continued

w	θ	y^a	y^s	y	w	θ	y^a	y^s	y	w	θ	y^a	y^s	y
1.470	1.70	10.40	9.88	.439	1.626	1.85	4.20	4.03	.161	1.758	1.10	6.55	6.16	.330
	1.60	12.12	11.51	.452		1.75	4.84	4.84	.202		1.90	7.47	7.00	.405
	1.50	13.97	13.24	.522		1.65	5.95	5.67	.245		.80	8.58	7.98	.516
	1.40	16.05	15.13	.643		1.55	6.93	6.59	.295		.70	9.89	9.17	.651
	1.30	18.34	17.44	.780		1.45	7.99	7.60	.355		.60	11.58	10.64	.854
	1.20	20.99	20.09	.955		1.35	9.12	8.64	.427		.60	13.76	12.58	1.11
	1.10	24.49	23.23	1.20		1.25	10.39	9.78	.510	1.800	2.25	.0165	.0160	.00059
	1.00	29.18	27.01	1.51		1.15	11.92	11.19	.627		2.15	.305	.297	.0105
	.90	34.53	31.79	1.96		1.05	13.75	12.83	.790		2.05	.691	.672	.0243
	.80	41.58	37.88	2.52		.95	15.86	14.78	1.005		.90	1.127	1.092	.0404
	.70	50.18	45.16	3.42		.85	18.59	17.16	1.31		.80	1.585	1.531	.0581
	.60	62.8	56.2	4.70		.75	22.03	20.22	1.68		.75	2.040	1.968	.0770
	.50	79.9	70.5	6.2		.65	26.63	24.16	2.30		.70	2.51	2.41	.0966
	.40	104.7	90.4	8.9		.55	32.26	28.89	3.17		.65	2.96	2.83	.119
	.30	142.9	118.2	13.7		.45	40.7	36.3	4.19		.60	3.41	3.25	.142
1.523	2.55	.0292	.0284	.00105	1.673	2.40	.0219	.0213	.00079		.85	3.90	3.70	.168
	2.45	.573	.564	.0197		2.30	.418	.408	.0144		.80	4.41	4.19	.199
	2.35	1.340	1.296	.0467		2.20	.963	.937	.0338		.75	4.95	4.68	.238
	2.25	2.235	2.165	.0799		2.10	1.546	1.546	.0571		.70	5.56	5.22	.282
	2.15	3.228	3.120	.1179		2.00	2.275	2.200	.0833		.95	6.32	5.92	.348
	2.05	4.276	4.188	.1606		1.90	2.978	2.872	.1121		.90	7.25	6.74	.443
	1.95	5.41	5.20	.208		1.80	3.72	3.57	.143		.75	8.35	7.74	.556
	1.85	6.57	6.31	.261		1.70	4.46	4.27	.178		.65	9.79	8.99	.736
	1.75	7.80	7.44	.321		1.60	5.22	4.98	.216	1.839	2.20	.0149	.0145	.00054
	1.65	9.17	8.71	.387		1.50	6.07	5.76	.259		2.10	.273	.266	.0094
	1.55	10.65	10.13	.469		1.40	6.96	6.62	.311		2.00	.616	.599	.0216
	1.45	12.23	11.59	.566		1.30	7.92	7.49	.372		.95	.999	.968	.0358
	1.35	14.02	13.22	.684		1.20	8.99	8.46	.444		.85	1.396	1.348	.0512
	1.25	16.16	15.20	.837		1.10	10.29	9.66	.546		.80	1.786	1.722	.0675
	1.15	18.71	17.47	1.05		1.00	11.85	11.05	.694		.70	2.18	2.09	.0843
	1.05	21.66	20.18	1.32		.90	13.68	12.74	.876		.50	2.56	2.45	.103
	.95	25.36	23.45	1.73		.80	16.02	14.76	1.15		.40	2.93	2.79	.123
	.85	30.01	27.61	2.22		.70	18.99	17.41	1.47		.30	3.33	3.16	.144
	.75	36.17	32.91	3.02		.60	23.00	20.83	2.02		.20	3.74	3.56	.171
	.65	43.72	39.27	4.17		.50	27.90	24.94	2.78		.10	4.18	3.95	.203
	.55	54.9	49.0	5.5	1.717	2.35	.0200	.0195	.00072		.00	4.68	4.39	.241
	.45	69.9	61.7	7.8		2.25	.378	.368	.0130	1.878	2.15	.0134	.0131	.00049
	.35	91.9	79.2	12.1		2.15	.866	.842	.0304		2.05	.243	.236	.0084
1.575	2.55	.0265	.0258	.0096	1.717	2.05	1.426	1.383	.0511		.95	.544	.529	.0191
	2.40	.517	.503	.0178		1.95	2.029	1.959	.0744		.85	.877	.850	.0315
	2.30	1.199	1.165	.0420		1.85	2.639	2.546	.0994		.75	1.218	1.177	.0447
	2.20	2.000	1.939	.0715		1.75	3.28	3.15	.126		1.75	1.546	1.493	.0597
	2.10	2.879	2.783	.1052		1.65	3.91	3.75	.157		1.65	1.88	1.80	.0725
	2.00	3.799	3.668	.1429		1.55	4.56	4.35	.189		1.55	2.18	2.09	.0884
	1.90	4.79	4.60	.183		1.45	5.27	5.01	.226		1.45	2.48	2.37	.104
	1.80	5.79	5.55	.231		1.35	6.03	5.73	.270		1.25	2.81	2.67	.122
	1.70	6.85	6.53	.282		1.25	6.82	6.46	.323		1.05	3.14	2.98	.144
	1.60	8.02	7.63	.339		1.15	7.72	7.26	.384		.95	3.49	3.30	.171
	1.50	9.28	8.82	.411		1.05	8.82	8.27	.473		.85	3.89	3.64	.202
	1.40	10.62	10.07	.494		.95	10.14	9.44	.600		.75	4.40	4.11	.249
	1.30	12.15	11.44	.593		.85	11.70	10.86	.760		.70	5.03	4.66	.318
	1.20	13.98	13.13	.729		.75	13.70	12.61	.994	1.914	2.10	.0127	.0119	.00044
	1.10	16.14	15.07	.914		.65	16.26	14.88	1.28		2.00	.217	.212	.0075
	1.00	18.66	17.38	1.16		.55	19.72	17.84	1.75		.90	.484	.471	.0171
	.90	21.85	20.19	1.52							.80	.776	.752	.0279
	.80	25.87	23.77	1.94							1.80	1.070	1.034	.0394
	.70	31.23	28.37	2.65							1.70	1.350	1.302	.0513
	.60	37.78	32.89	3.65							1.50	1.63	1.56	.0629
	.50	47.5	42.4	4.75							1.30	1.88	1.80	.0762
	.40	60.8	53.5	6.91							1.20	2.12	2.01	.0896
1.626	2.45	.0240	.0233	.0087							1.30	2.38	2.26	.104
	2.35	.462	.450	.0159							1.20	2.64	2.51	.123
	2.25	1.067	1.037	.0374										
	.60	1.773	1.720	.0634										
	.50	2.541	2.457	.0930										
	.05	3.339	3.224	.1257										

TABLE II.- Ψ^a, Ψ^s, AND Ψ AS FUNCTIONS OF w AND θ ($A^a = 100$, $A^s = 1000$, $\gamma = 1.405$) - Concluded
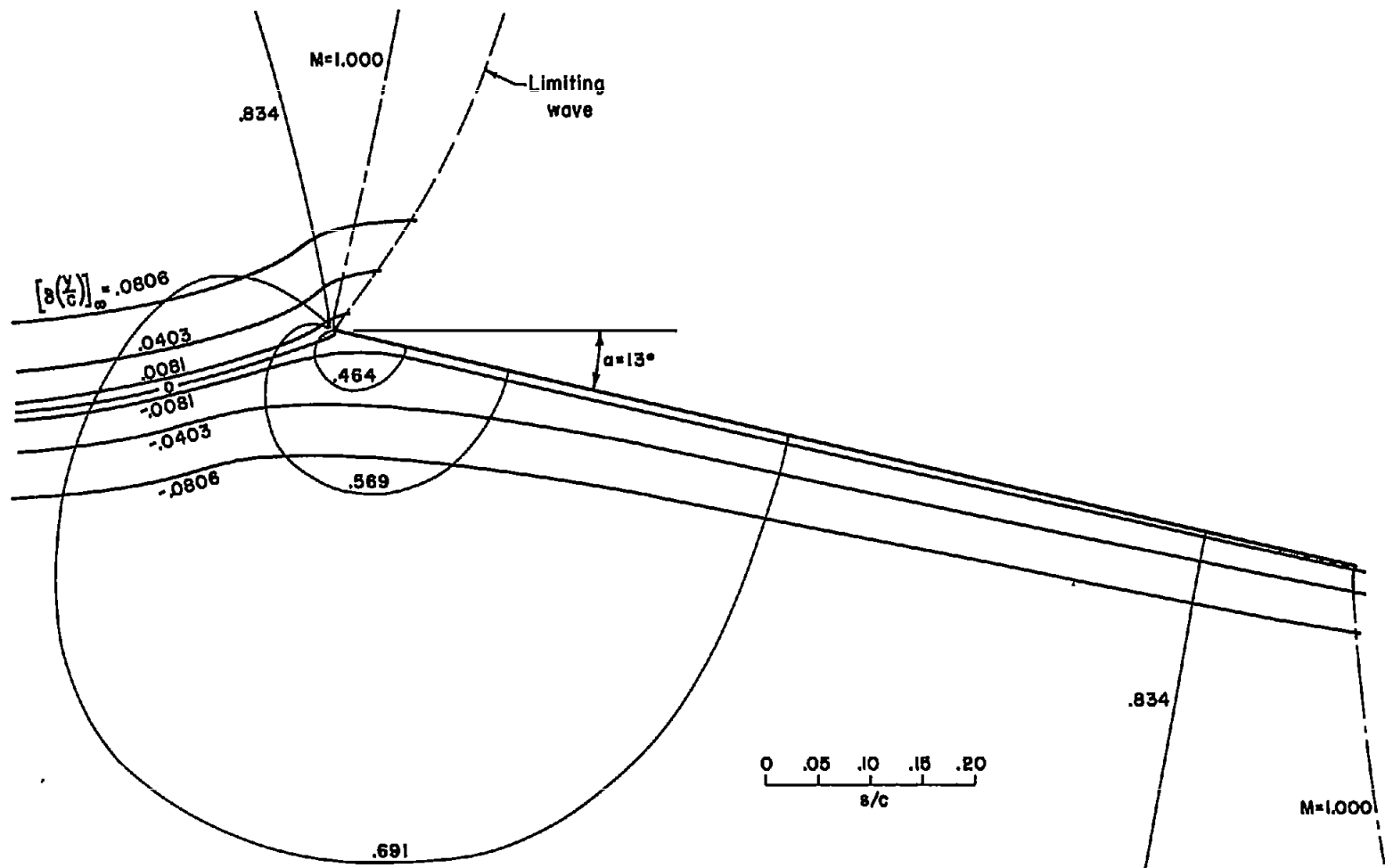
w	θ	Ψ^a	Ψ^s	Ψ	w	θ	Ψ^a	Ψ^s	Ψ
1.914	1.00	2.92	2.75	.145	2.077	1.85	.0070	.0068	.00025
	.90	3.23	3.03	.171		1.75	.116	.113	.0041
	.80	3.65	3.41	.211		1.65	.249	.242	.0088
1.950	2.05	.0110	.0107	.00039		1.55	.382	.371	.0138
	1.95	.193	.188	.0067		1.45	.504	.487	.0187
	1.85	.428	.416	.0151		1.35	.605	.584	.0232
	1.75	.680	.659	.0245		1.25	.69	.67	.0270
	1.65	.931	.900	.0343		1.15	.76	.73	.0318
	1.55	1.166	1.124	.0443		1.05	.81	.77	.0359
	1.45	1.39	1.34	.0540	2.106	1.80	.0061	.0059	.00022
	1.35	1.59	1.53	.0650		1.70	.100	.097	.0035
	1.25	1.78	1.70	.0758		1.60	.211	.206	.0075
	1.15	1.99	1.88	.0878		1.50	.321	.311	.0116
	1.05	2.19	2.08	.103		1.40	.418	.404	.0155
	.95	2.40	2.27	.121		1.30	.496	.478	.0191
	.85	2.65	2.48	.143		1.20	.56	.54	.0220
1.983	2.00	.0099	.0096	.00036		1.10	.60	.58	.0257
	1.90	.172	.168	.0060	2.133	1.75	.0054	.0052	.00019
	1.80	.378	.368	.0134		1.65	.085	.083	.0030
	1.70	.597	.579	.0215		1.55	.178	.174	.0063
	1.60	.811	.784	.0299		1.45	.268	.260	.0097
	1.50	1.007	.971	.0384		1.35	.344	.333	.0128
	1.40	1.19	1.14	.0463		1.25	.401	.387	.0155
	1.30	1.35	1.29	.0552		1.15	.444	.43	.0178
	1.20	1.50	1.43	.0641					
	1.10	1.65	1.57	.0737	2.161	1.70	.0046	.0045	.00017
	1.00	1.81	1.72	.0861		1.60	.072	.070	.0025
	.90	1.97	1.86	.101		1.50	.149	.145	.0053
						1.40	.214	.214	.0080
						1.30	.278	.269	.0104
2.016	1.95	.0088	.0086	.00032		1.20	.318	.307	.0124
	1.85	.151	.147	.0053					
	1.75	.330	.321	.0117	2.187	1.65	.0040	.0038	.00014
	1.65	.516	.501	.0187		1.55	.060	.059	.0021
	1.55	.695	.672	.0257		1.45	.124	.120	.0044
	1.45	.855	.824	.0326		1.35	.179	.174	.0065
	1.35	1.00	.96	.0388		1.25	.223	.215	.0083
	1.25	1.12	1.08	.0462					
	1.15	1.23	1.17	.0532	2.211	1.60	.0034	.0034	.00012
	1.05	1.35	1.28	.0608		1.50	.051	.049	.0018
	.95	1.46	1.39	.0707		1.40	.102	.099	.0036
						1.30	.145	.141	.0053
2.046	1.90	.0079	.0077	.00028					
	1.80	.133	.130	.0047	2.234	1.55	.0029	.0028	.00011
	1.70	.288	.281	.0102		1.45	.041	.040	.0015
	1.60	.447	.434	.0162		1.35	.081	.079	.0029
	1.50	.596	.576	.0221					
	1.40	.726	.699	.0278					
	1.30	.84	.81	.0327	2.257	1.50	.0024	.0023	.00009
	1.20	.93	.89	.0386		1.40	.033	.032	.0012
	1.10	1.01	.96	.0441					
	1.00	1.09	1.04	.0500	2.280	1.45	.0020	.0019	.00007

TABLE III.- x/c AND y/c AS FUNCTIONS OF r ON LIMITING CHARACTERISTIC.

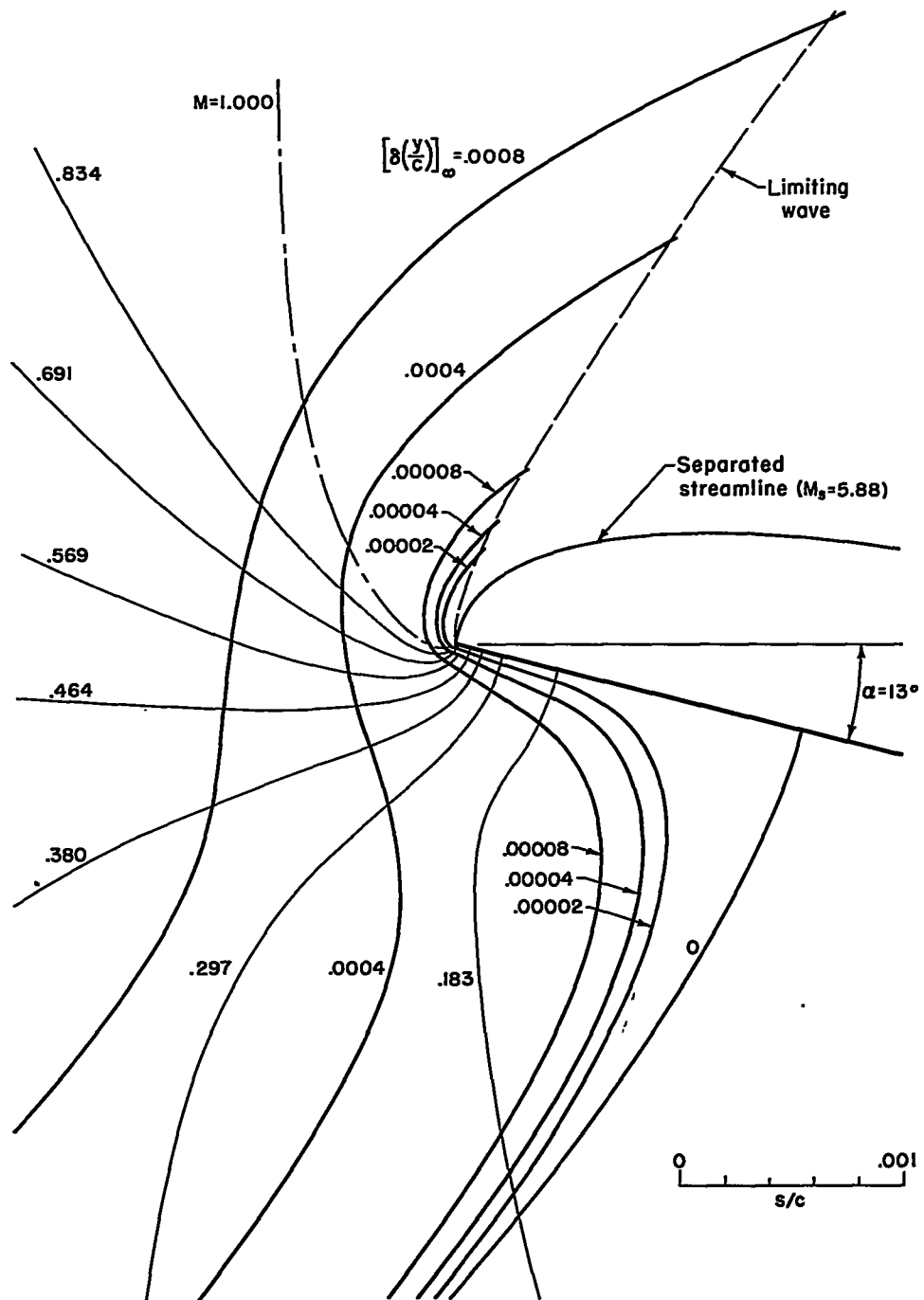| r	(x/c)	(y/c)
2.9	-0.087×10^{-6}	1.667×10^{-6}
2.8	$-.665 \times 10^{-6}$	21.40×10^{-6}
2.7	$-.552 \times 10^{-6}$	44.60×10^{-6}
2.6	$.394 \times 10^{-6}$	67.20×10^{-6}
2.5	2.127×10^{-6}	88.57×10^{-6}
2.4	4.648×10^{-6}	110.15×10^{-6}
2.3	7.911×10^{-6}	131.6×10^{-6}
2.2	12.53×10^{-6}	155.8×10^{-6}
2.1	18.02×10^{-6}	179.9×10^{-6}
2.0	24.97×10^{-6}	206.3×10^{-6}
1.9	34.25×10^{-6}	237.3×10^{-6}
1.8	46.76×10^{-6}	273.9×10^{-6}
1.7	62.54×10^{-6}	315.4×10^{-6}
1.6	85.45×10^{-6}	371.4×10^{-6}
1.5	118.18×10^{-6}	443.9×10^{-6}
1.4	161.65×10^{-6}	533.7×10^{-6}
1.3	223.73×10^{-6}	653.6×10^{-6}
1.2	301.87×10^{-6}	791.3×10^{-6}
1.1	433.60×10^{-6}	1008.1×10^{-6}
1.0	616.2×10^{-6}	1298.4×10^{-6}
.9	8.330×10^{-4}	16.359×10^{-4}
.8	12.05×10^{-4}	21.933×10^{-4}
.7	18.52×10^{-4}	31.01×10^{-4}
.6	31.38×10^{-4}	49.02×10^{-4}
.5	55.68×10^{-4}	81.91×10^{-4}
.45	74.34×10^{-4}	107.0×10^{-4}
.4	102.59×10^{-4}	145.4×10^{-4}
.35	144.01×10^{-4}	202.6×10^{-4}
.3	208.0×10^{-4}	292.4×10^{-4}
.25	324.2×10^{-4}	457.1×10^{-4}
.2	529.4×10^{-4}	766.0×10^{-4}
.15	957.7×10^{-4}	1444.7×10^{-4}

(a) Complete plate.

Figure 1.- Flow field.

M=1.000

.834

.691

← Limiting wave

.569

$\left[\delta\left(\dfrac{y}{c}\right)\right]_\infty = .0081$

Separated streamline ($M_s = 5.88$)

P

$\alpha = 13°$

.0040

.183

.0008

0

-.0008

.297
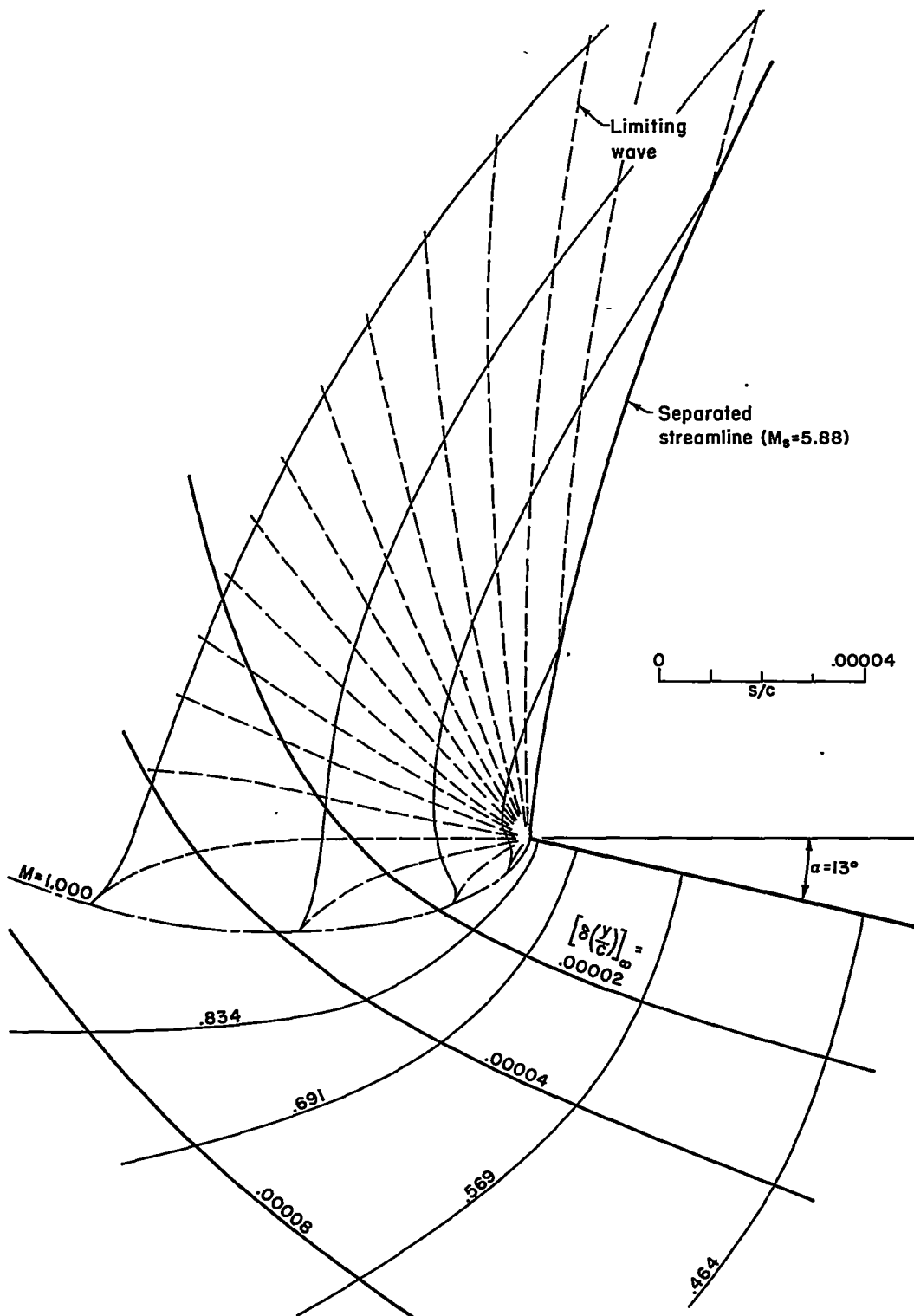
.005   .01
s/c

-.0040
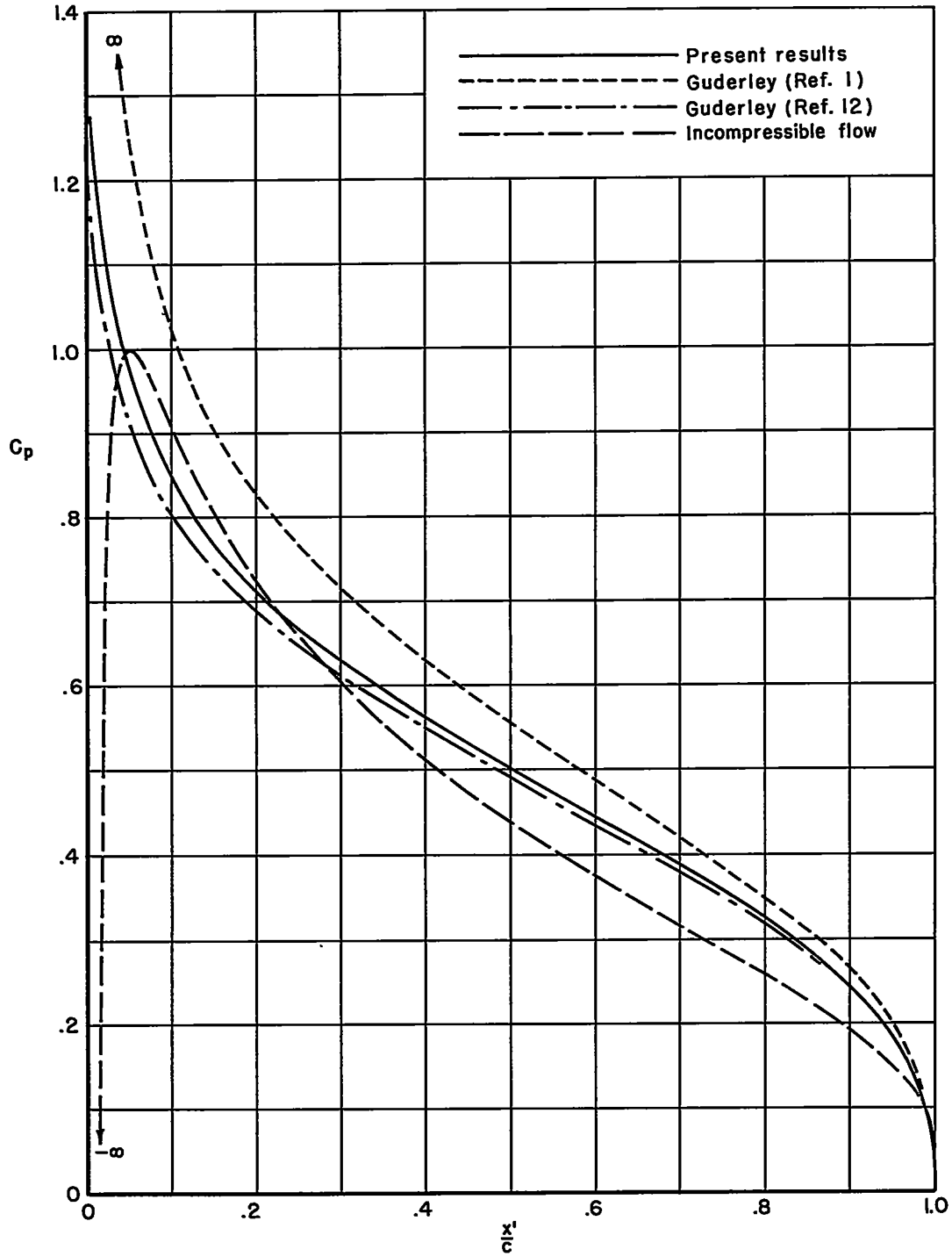
.380

M=.464

.380
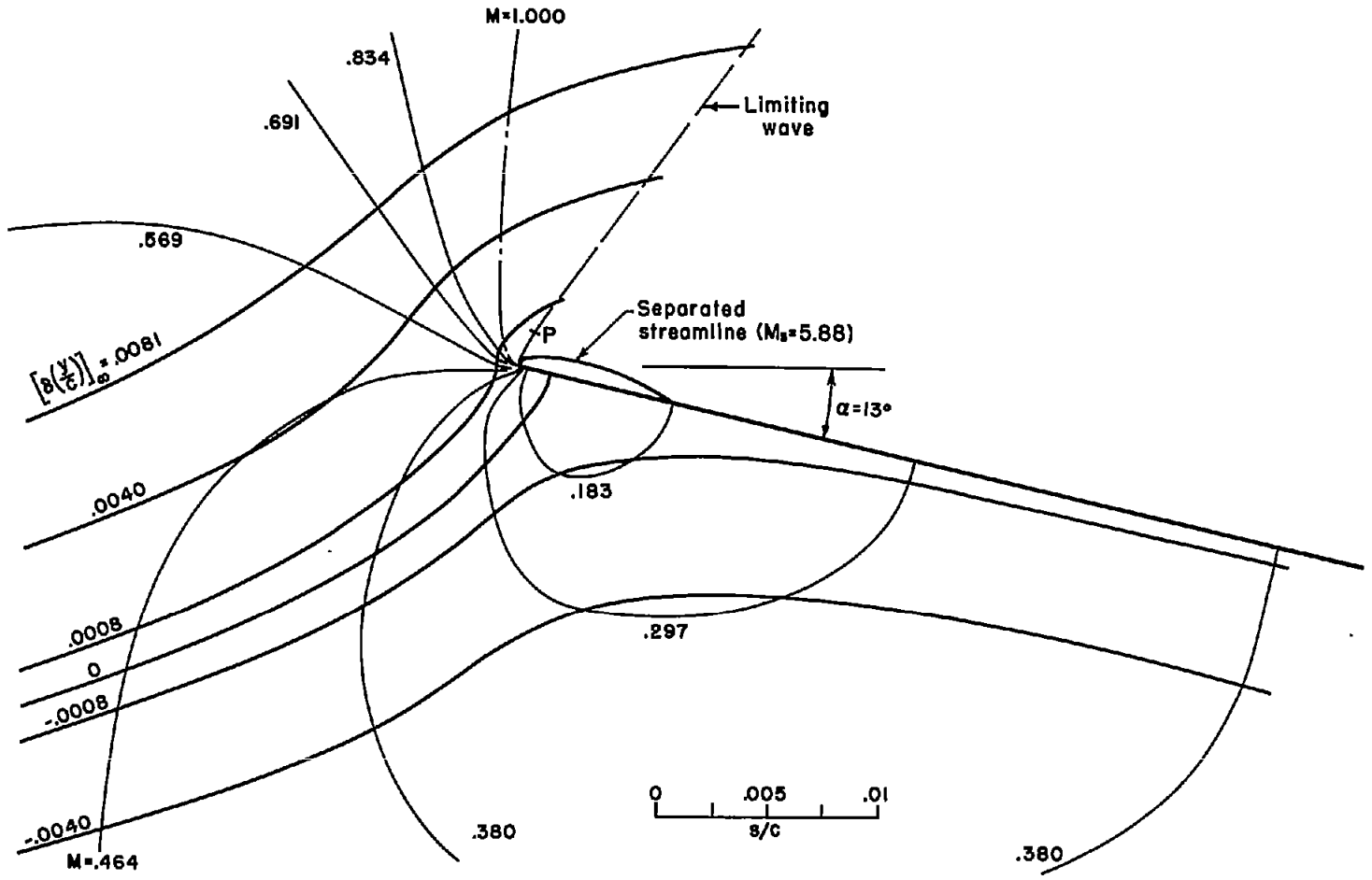
(b) Forward portion of plate.

Figure 1.- Continued.

(c) Vicinity of stagnation point.

Figure 1.- Continued.

(d) Vicinity of leading edge.

Figure 1.- Concluded.

(a) Complete plate.

Figure 2.- Lower surface pressure distribution.
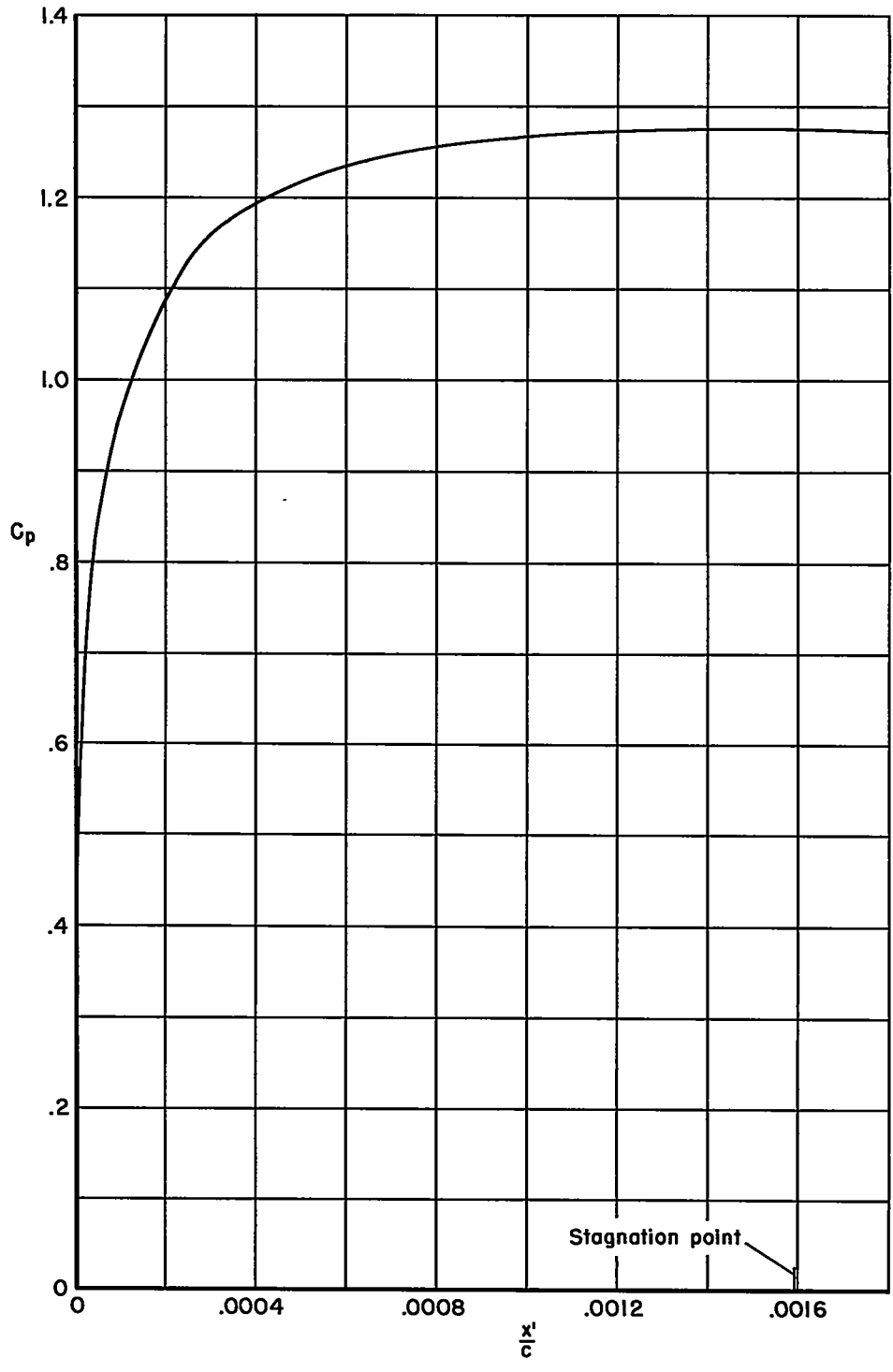
(b) Vicinity of leading edge.

Figure 2.- Concluded.
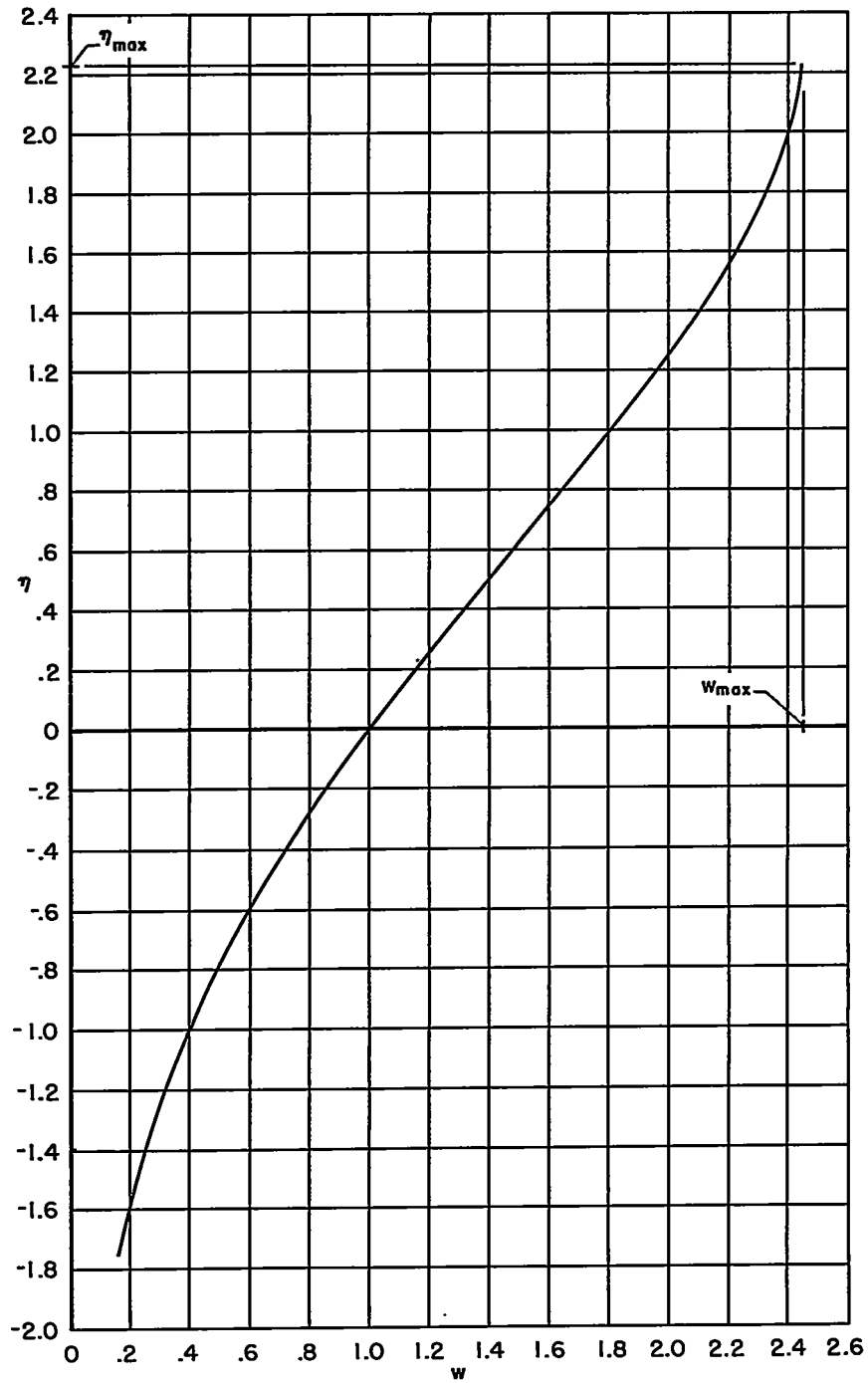
Figure 3.- η as a function of w.
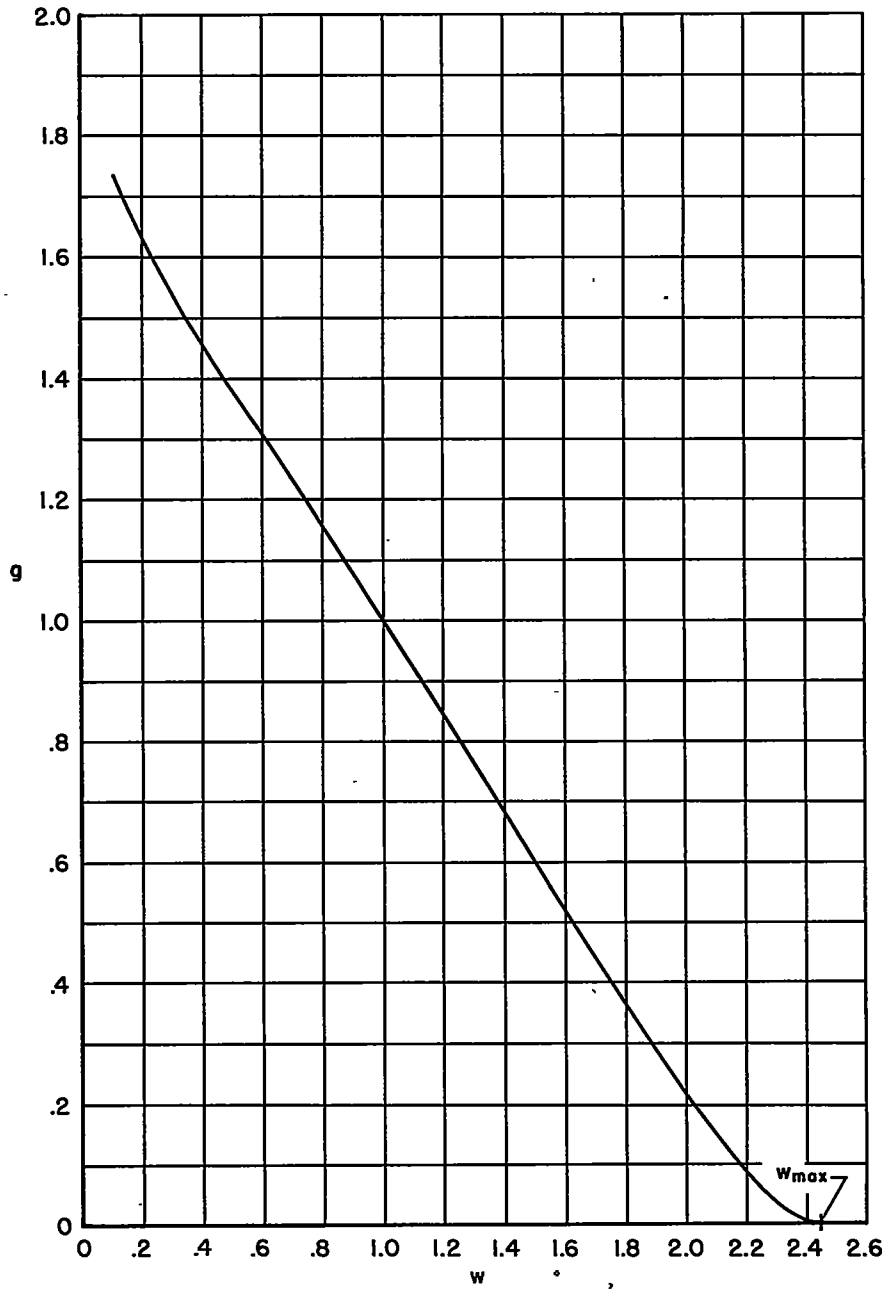
Figure 4.- g as a function of w.
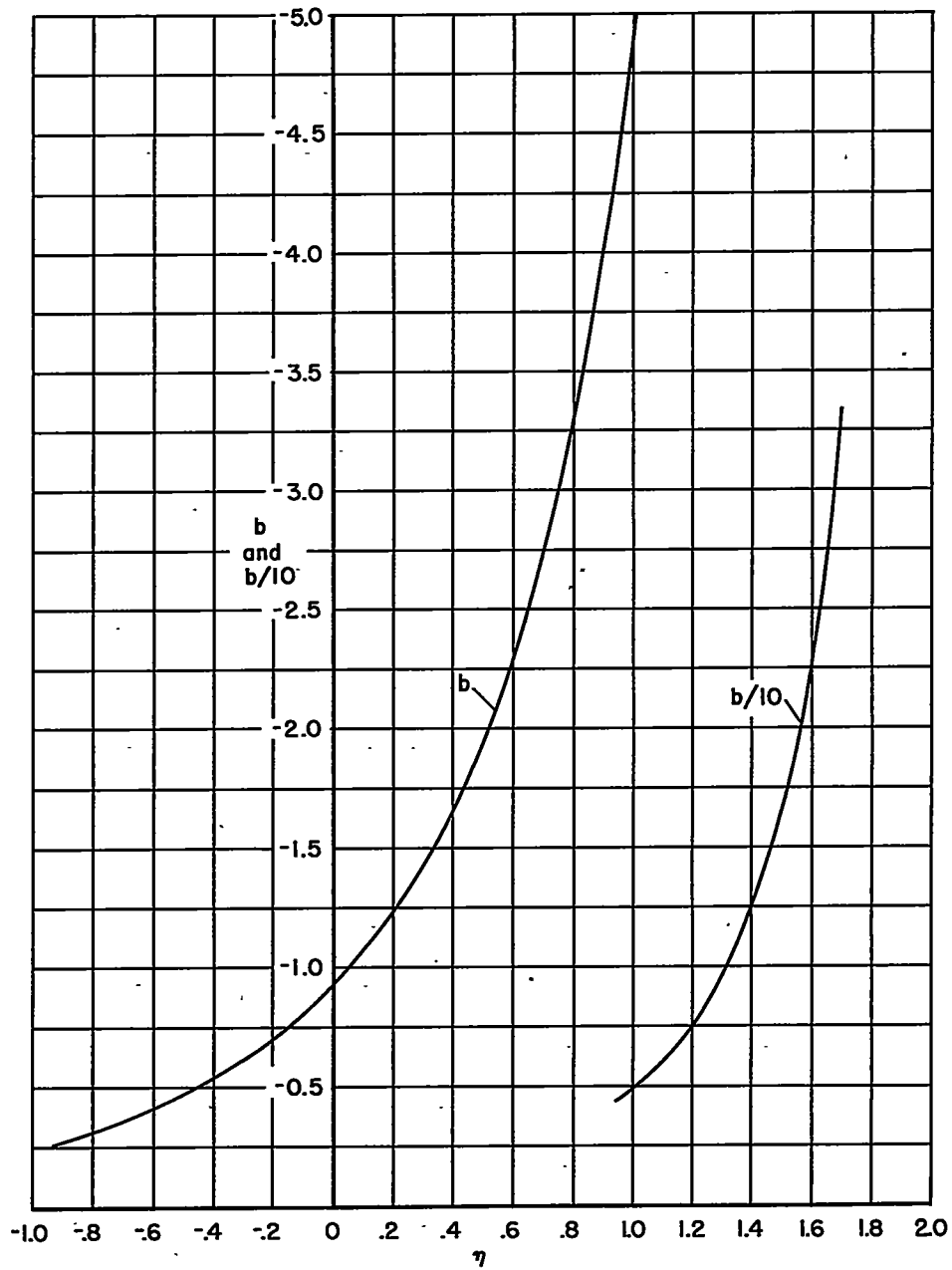
Figure 5.- b as a function of η.
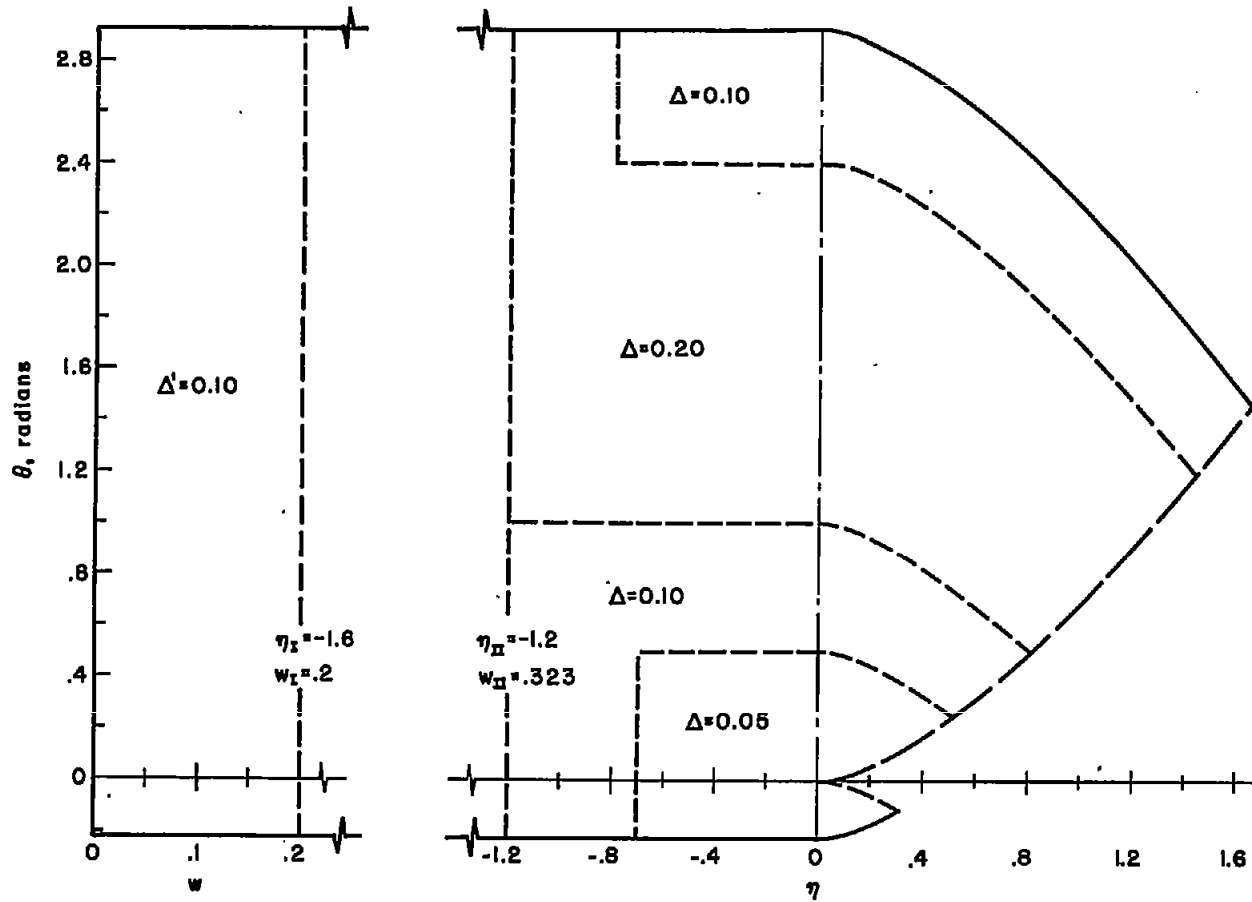
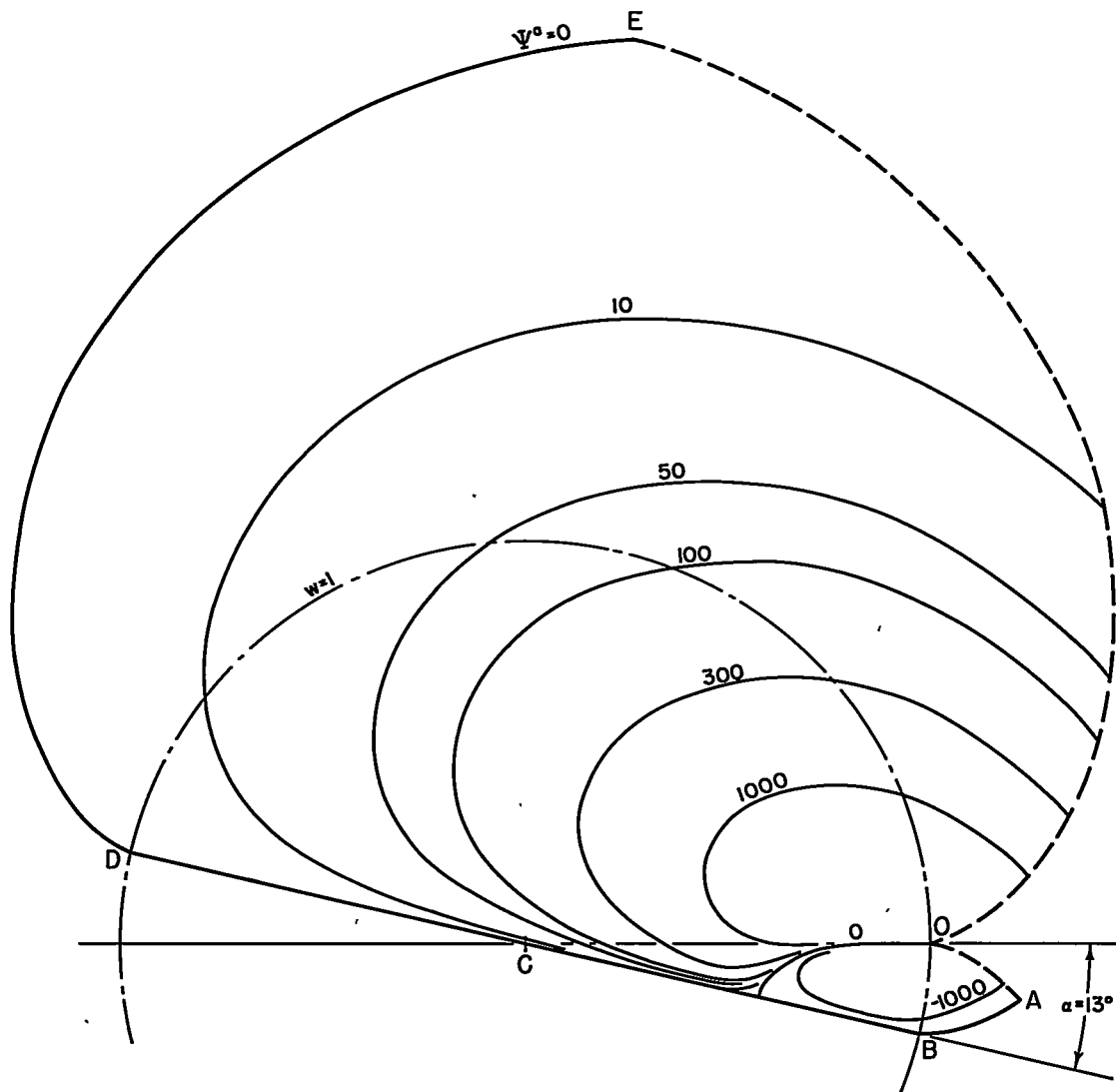Figure 6.- Distribution of mesh interval for calculated example ($\alpha = 13^{\circ}$).

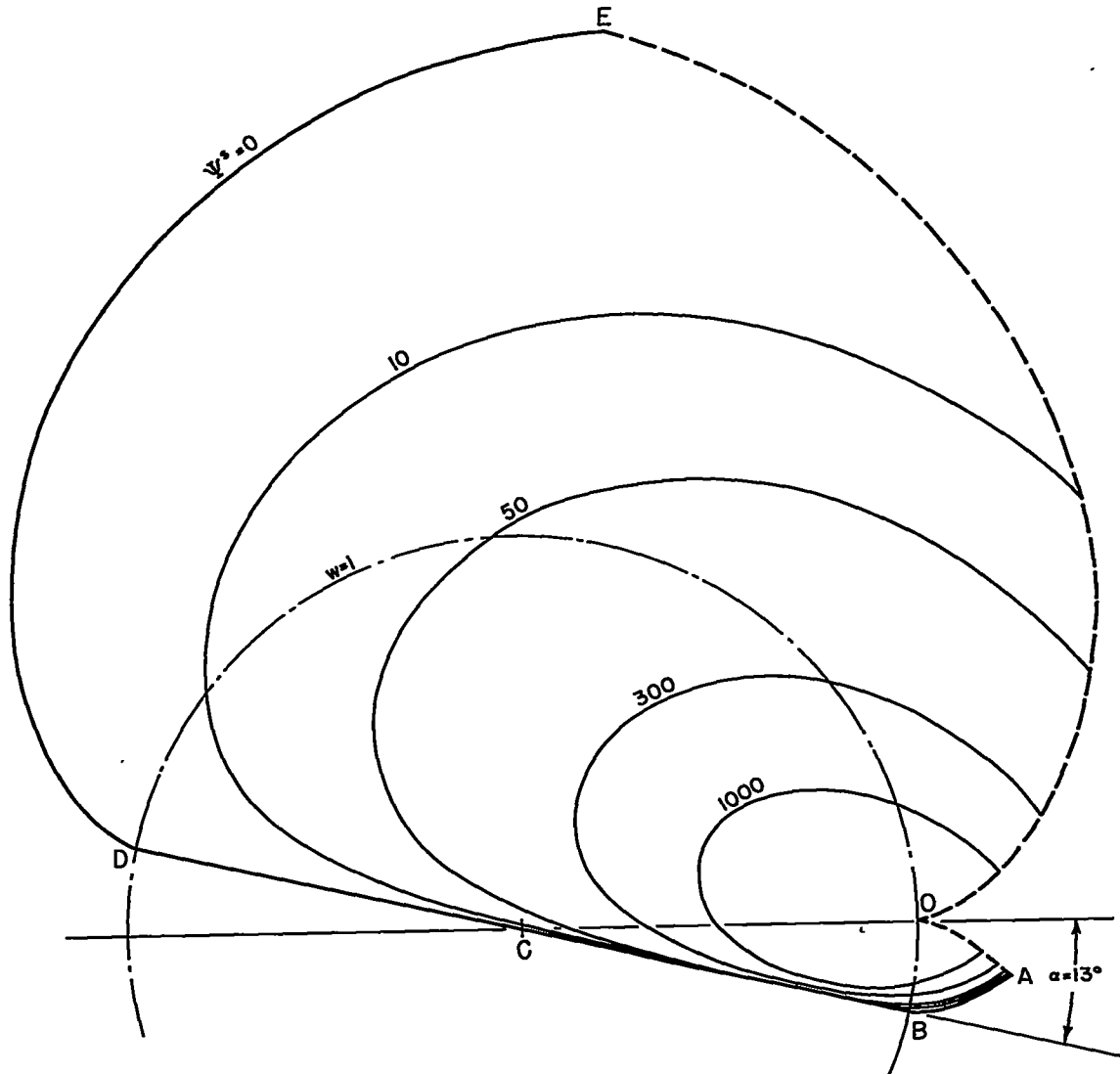Figure 7.- Contour map of Ψ^a in w,θ coordinates ($A^a = 100$, $\gamma = 1.405$).

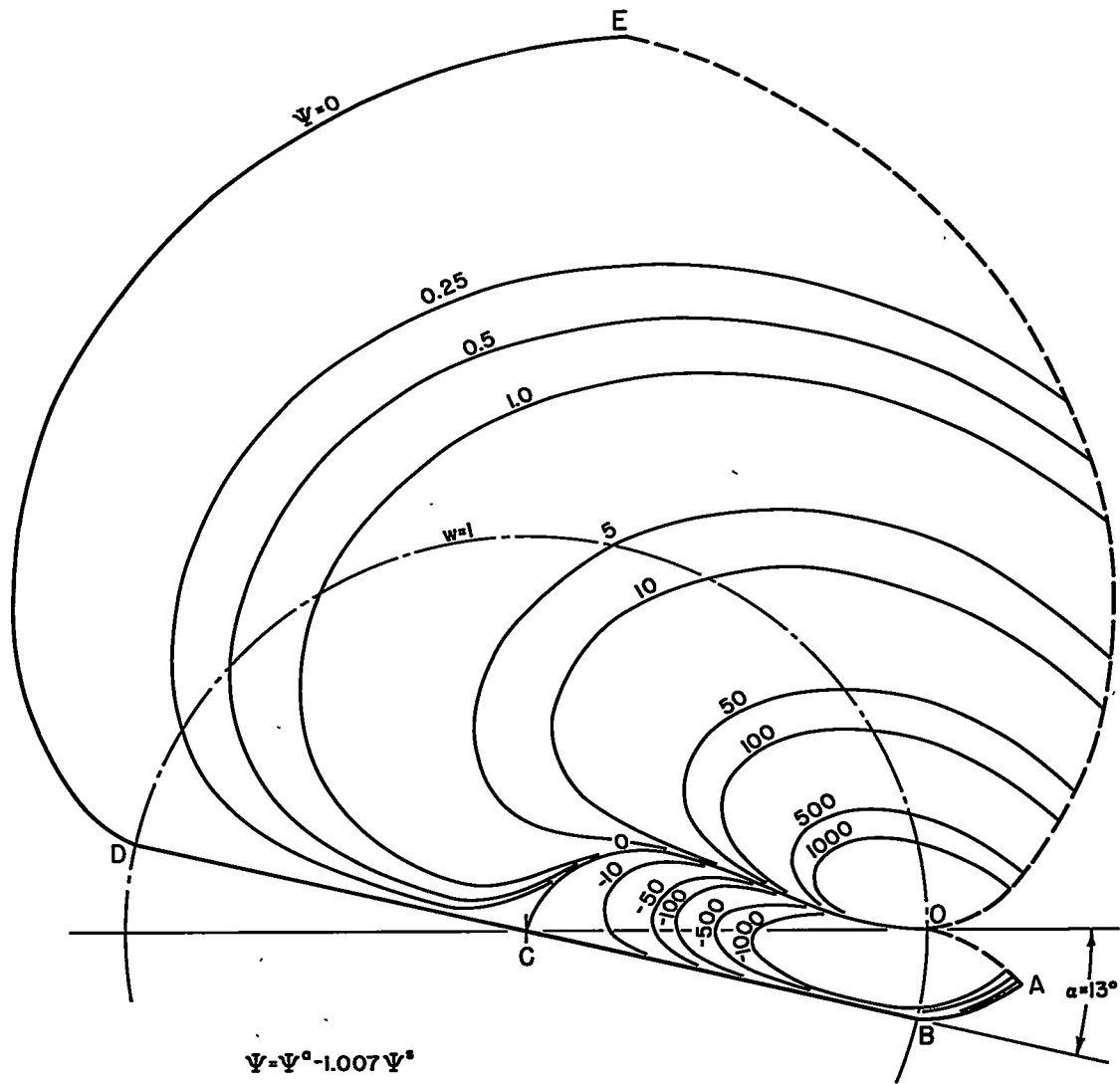Figure 8.- Contour map of Ψ^s in w,θ coordinates $(A^s = 1000, \gamma = 1.405)$.

Figure 9.- Contour map of Ψ in w,θ coordinates ($\gamma = 1.405$).